

## Article

# Hydrodesulfurization of Thiophene in *n*-Heptane Stream Using CoMo/SBA-15 and CoMo/AlSBA-15 Mesoporous Catalysts

Ana Carla S. L. S. Coutinho<sup>1</sup>, Joana M. F. Barros<sup>2</sup>, Marcio D. S. Araujo<sup>3</sup>, Jilliano B. Silva<sup>4</sup>, Marcelo J. B. Souza<sup>5</sup>, Regina C. O. B. Delgado<sup>6</sup>, Valter J. Fernandes Jr.<sup>7</sup> and Antonio S. Araujo<sup>8,\*</sup>

- <sup>1</sup> School of Engineering, Fluminense Federal University, Niteroi 24210-253, RJ, Brazil; acoutinho@id.uff.br  
<sup>2</sup> Academic Unit of Biology and Chemistry, Center of Education and Health, Federal University of Campina Grande, Cuite 58175-000, PB, Brazil; joana.maria@professor.ufcg.edu.br  
<sup>3</sup> Institute of Chemistry, Federal University of Rio Grande do Norte, Natal 59078-970, RN, Brazil; marcio.ifrn@gmail.com  
<sup>4</sup> Post-Graduate Program in Petroleum and Energy, Federal University of Rio Grande do Norte, Natal 59078-970, RN, Brazil; jilliano.lcl@gmail.com  
<sup>5</sup> Department of Chemical Engineering, Federal University of Sergipe, Sao Cristovao 59078-970, SE, Brazil; marcelojbs@ufs.br  
<sup>6</sup> Department of Engineering and Technology, Federal Rural University of Semi-Arid, Mossoro 59625-900, RN, Brazil; regina.brasil@ufersa.edu.br  
<sup>7</sup> Laboratory of Fuels and Lubricants, Institute of Chemistry, Federal University of Rio Grande do Norte, Natal 59078-970, RN, Brazil; valter.fernandes@ufrn.br  
<sup>8</sup> Laboratory of Catalysis and Petrochemistry, Institute of Chemistry, Federal University of Rio Grande do Norte, Natal 59078-970, RN, Brazil  
\* Correspondence: antonio.araujo@ufrn.br



**Citation:** Coutinho, A.C.S.L.S.; Barros, J.M.F.; Araujo, M.D.S.; Silva, J.B.; Souza, M.J.B.; Delgado, R.C.O.B.; Fernandes Jr., V.J.; Araujo, A.S. Hydrodesulfurization of Thiophene in *n*-Heptane Stream Using CoMo/SBA-15 and CoMo/AlSBA-15 Mesoporous Catalysts. *Catalysts* **2024**, *14*, 198. <https://doi.org/10.3390/catal14030198>

Academic Editor: Narendra Kumar

Received: 20 January 2024

Revised: 25 February 2024

Accepted: 28 February 2024

Published: 18 March 2024



**Copyright:** © 2024 by the authors. Licensee MDPI, Basel, Switzerland. This article is an open access article distributed under the terms and conditions of the Creative Commons Attribution (CC BY) license (<https://creativecommons.org/licenses/by/4.0/>).

**Abstract:** Heterogeneous catalysts containing cobalt and molybdenum supported on mesoporous materials types SBA-15 and AlSBA-15 were synthesized for application in the HDS reactions of thiophene in the *n*-heptane stream. The materials were synthesized by the hydrothermal method using Pluronic P123 as a template. The calcined SBA-15 and AlSBA-15 supports were submitted to co-impregnation with solutions of cobalt nitrate and ammonium heptamolybdate, aiming for the production of 15% in mass of metal loading with an atomic ratio of  $[Co/(Co + Mo)] = 0.45$ . The obtained materials were dried and calcined to obtain the mesoporous catalysts in the forms of CoMo/SBA-15 and CoMo/AlSBA-15. The catalysts were characterized by XRD, TG/DTG, SEM, and nitrogen adsorption. From XRD analysis, it was verified that after the decomposition of the cobalt and molybdenum salts,  $MoO_3$ ,  $Co_3O_4$ , and  $CoMoO_4$  oxides were formed on the supports, being attributed to these chemical species, the activity for the HDS reactions. The catalytic activity of the obtained catalysts was evaluated in a continuously flowing tubular fixed-bed microreactor coupled on-line to a gas chromatograph, using an *n*-heptane stream containing 12,070 ppm of thiophene (ca. 5100 ppm of sulfur) as a model compound. The synthesized catalysts presented suitable activity for the HDS reaction, and the main obtained products were *cis*- and *trans*-2-butene, 1-butene, *n*-butane, and low amounts of isobutane. The presence of 1,3-butadiene and tetrahydrothiophene (THT) was not detected. A mechanism of the primary and secondary reactions and subsequent formation of the olefins and paraffins in the CoMo/SBA-15 and CoMo/AlSBA-15 mesoporous catalysts was proposed, considering steps of desulfurization, hydrogenation, dehydrogenation, THT decyclization, and isomerization.

**Keywords:** SBA-15; nanostructured materials; cobalt; molybdenum; hydrodesulfurization; environmental catalysis; petroleum refining

## 1. Introduction

The removal of sulfur from fossil fuels is one of the most important processes in modern refineries. It is accomplished via hydrodesulfurization (HDS) of the sulfur organic

compounds in the presence of heterogeneous catalysts. Currently, to comply with environmental legislation in many countries, there is great interest in developing processes to remove atmospheric contaminants, mainly sulfur derivatives, in addition to other hydrotreatment reactions. Classical catalysts used for such reactions in refining crude oil or liquid fuels generally consist of molybdenum supported on high surface area aluminas containing cobalt or nickel as promoters.

Hydrotreating processes (HDT) were developed from hydrogenation and cracking processes, and the most important HDT reaction was the removal of sulfur from the various fractions of petroleum and liquid coal derivatives, a process called hydrodesulfurization (HDS). Catalytic hydrotreatment consists of a variety of hydrogenation processes where oil and its various fractions react catalytically with hydrogen to remove S, N, O, and metals. Nowadays, hydrotreating is widely used to convert heavy oil loads and to improve the quality of various products. It is used in the pretreatment of charges for other refining processes such as catalytic reforming, catalytic cracking (FCC), and hydrocracking catalyst (HCC). Such pretreatment aims, among others, to protect the catalysts used in many consecutive stages in refining processes; reduce  $\text{NO}_x$  and  $\text{SO}_x$  emissions that may appear in the combustion of organic molecules, thus preventing premature corrosion of equipment; promote the improvement of the final properties of products from refineries (color, smell, stability, etc.); and add value to heavy distillates [1–3].

The use of increasingly heavier loads requires, in addition to hydrodesulfurization, conversion of larger molecules into smaller ones (hydrocracking—HCC) and removal of metals (hydrodemetallization—HDM), nitrogen (hydrodenitrogenation—HDN), and, in some cases, oxygen (hydrodeoxygenation—HDO). With the development of the petrochemical industry, other processes also gained prominence, such as aromatics degradation: hydrodearomatization (HDA); interconversion of organic molecules: isomerization (ISM); breaking of C-C bonds: hydrocracking (HCC); and olefin saturation: hydrogenation (HYD). Purification processes using hydrogen are applied to practically all distillate fractions. The complexity of the load and the lack of detailed knowledge about the nature of the compounds present in crude oil are two of the difficulties of hydrotreatment. It can be said that petroleum contains mainly hydrocarbons and, depending on its origin, may also contain large concentrations of heteroatoms [4–6].

The most industrially used HDS catalysts are based on  $\text{Co}(\text{Ni})\text{Mo}/\text{Al}_2\text{O}_3$ , which have high mechanical strength and a large specific surface area [7–9]. The strong interactions between metals and alumina promote the formation of Mo-O-Al phases, resulting in an active phase for the process [10,11]. However, the phase formation between Co/Ni and  $\text{Al}_2\text{O}_3$  is unfavorable for regulating the catalytic performance of  $\text{MoS}_2$  sites. Active metal loading and unfavorable interactions have limited supported HDS catalysts to produce ultra-low sulfur fuels. Thus, several studies have been carried out aiming to improve the performance of HDS in relation to the following aspects: modification of zeolite supports, such as ZSM-5 [12–14] and Y zeolite [15], materials based on mesoporous silica, such as MCM-41, SBA-15, and SBA-16 [16–19], oxides single and mixed metallic [20–26], and carbon-based materials [27–33]. However, the development of new catalysts containing well-defined micro- and mesopores requires further research and additional modifications for evaluation as new supports for ultra-deep desulfurization.

The advantage of HDS over oxidative or adsorptive desulfurization methods lies in its effectiveness in removing a wide range of sulfur compounds from hydrocarbon streams at relatively mild conditions. HDS operates at high temperatures and pressures, typically using metal catalysts such as molybdenum or cobalt, which enables the efficient removal of sulfur compounds, including thiols, sulfides, and thiophenes. This method is effective in reducing sulfur content to meet stringent environmental regulations, and it does not produce harmful waste products as in some oxidative methods. Additionally, HDS is well suited for treating a wide variety of feedstocks, making it a versatile and widely used desulfurization method in the petroleum industry. Specifically, some of the key advantages of HDS include selectivity, efficiency, and compatibility with existing

infrastructure. HDS is highly selective for sulfur removal, allowing for the removal of sulfur compounds without significantly affecting the hydrocarbon components. This selectivity is crucial for refining high-quality fuels. HDS processes can achieve high desulfurization efficiency, even at relatively mild operating conditions, which can result in lower energy consumption compared to other methods. These advantages make HDS a popular choice for desulfurization in the petroleum refining industry.

The composition of the hydrotreatment charge varies widely depending on the origin of the oil. Sulfur is the most abundant of the heteroatoms present in crude oil, in general, ranging from 0.1 to 5% *w/w*. The content of nitrogen compounds present in petroleum varies from 0.1 to 1% *w/w* and is generally concentrated in the heaviest fractions, mainly containing pyridine nuclei. Oxygen compounds are generally present in smaller quantities, values below 0.1% *w/w*, and are found in the forms of carboxylic acids and phenols. In Figure 1, some of the different types of aromatic compounds and sulfur-containing compounds commonly found in crude oil fractions are presented. The need to use increasingly heavier loads has led several countries in America and the European Union to increase efforts to control and prevent the emission of these pollutants. Thus, policies regulating the amounts of toxic compounds in fuels from refineries are being established. In Brazil, the National Agency of Petroleum, Natural Gas and Biofuels controls the concentration of sulfur in oil, gas, and fuels.

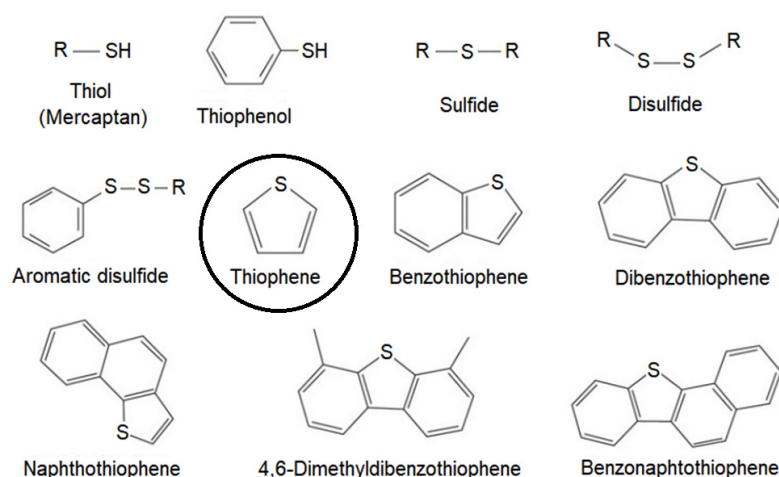


**Figure 1.** Some typical aromatic compounds and sulfur-containing compounds found in petroleum fractions, highlighting the molecular structure of thiophene.

Thiophene is a highly reactive molecule that contains a five-membered ring consisting of four carbon atoms and one sulfur atom. Thiophene readily undergoes various reactions, including nucleophilic and electrophilic substitutions, cyclization, and oxidation. For this reason, it was chosen as a probe molecule for this research.

Thiophene is commonly used in hydrodesulfurization (HDS) research for several specific/scientific reasons: (i) Thiophene is a heterocyclic compound containing sulfur, which is structurally similar to many sulfur-containing compounds found in crude oil; therefore, studying thiophene allows researchers to understand the behavior of more complex sulfur-containing compounds found in petroleum. (ii) Thiophene serves as a model compound for studying the mechanisms and kinetics of hydrodesulfurization reactions. Its relatively simple structure makes it suitable for detailed experimental and theoretical investigations, providing insights into the fundamental processes involved in HDS reactions. (iii) Researchers use thiophene as a probe molecule to evaluate the performance of various catalysts in hydrodesulfurization processes. Thus, by studying the effect of different catalysts on the conversion of thiophene to its desulfurized products, it is possible to identify catalysts with improved activity, selectivity, and stability for industrial HDS applications. Thiophene is also employed in mechanistic studies aimed at

understanding the detailed reaction pathways involved in hydrodesulfurization. The use of thiophene in hydrodesulfurization research allows us to elucidate fundamental principles concerning sulfur removal from fossil fuels, leading to the development of more efficient and environmentally friendly HDS processes.

This work aimed to propose the synthesis of hydrodesulfurization catalysts (HDS) based on mesoporous molecular sieves of the SBA-15 and AISBA-15 containing cobalt and molybdenum oxides deposited on their surface. Typically, SBA-15-type mesoporous materials have a high specific surface area and large pore diameter, perfectly adaptable to the kinetic diameters of the largest sulfur compound molecules. These structural characteristics of the support are fundamental to maximizing the metal dispersion of the active phases as well as improving the accessibility of the largest sulfur compounds, like thiophene, to metal sites, improving the efficiency of HDS processes.

## 2. Results and Discussion

### 2.1. Thermal Analysis of the Supports and Catalysts

Heat treatment or calcination is a very important step in obtaining high-quality SBA-15 and AISBA-15 mesoporous materials. In this step, all the P123 triblock copolymers used as a structure template are removed. Thermogravimetry is a technique used to determine the best calcination conditions, aiming to remove all organic material and preserve the well-ordered hexagonal structure. Figure 2 shows the TG and DTG curves for the SBA-15 and AISBA-15 samples in the non-calcined form at three different heating rates ( $\beta = 5, 10,$  and  $20\text{ }^{\circ}\text{C}/\text{min}$ ).

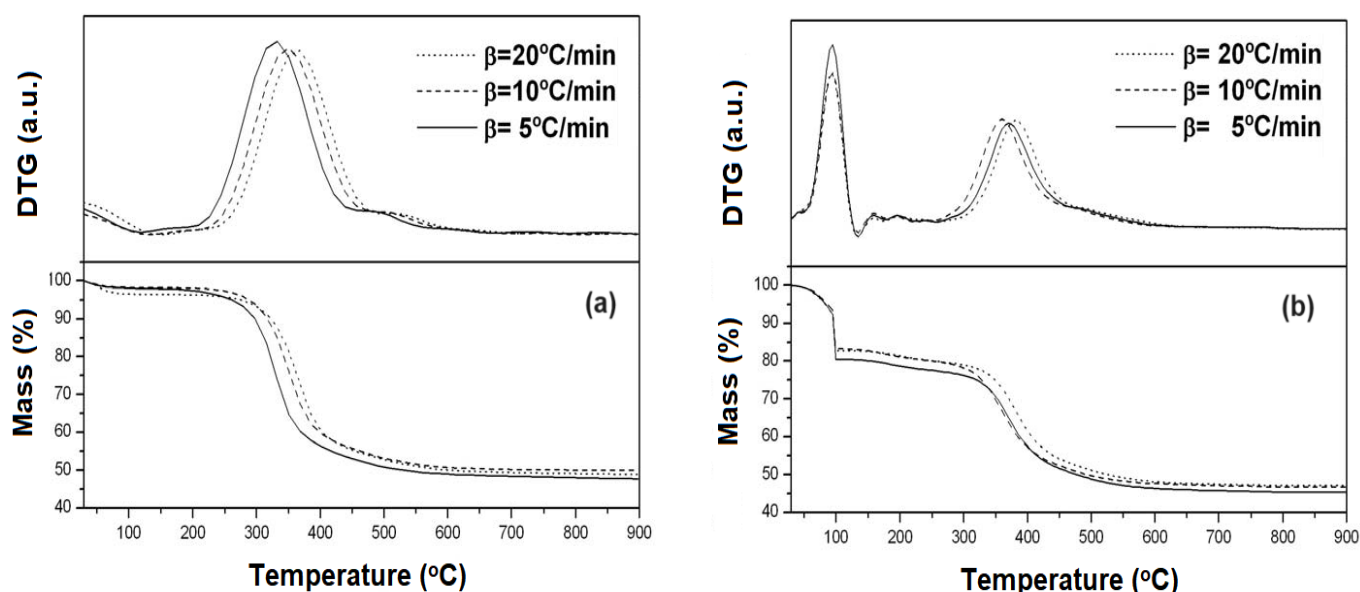


**Figure 2.** Thermogravimetry (TG) and derivative thermogravimetry (DTG) curves for the mesoporous supports at different heating rates: (a) SBA-15 and (b) AISBA-15.

As can be seen from the TG/DTG curves, three mass loss events were typically obtained (Table 1). These events are attributed to (i) range of 30–130 °C, desorption of physisorbed water in the pores of the material; (ii) range of 130–450 °C, removal of the directing molecules (P123); and (iii) range of 450–650 °C, residual removal of template and release of interstitial water resulting from the silanol condensation process. This behavior is typical for mesoporous materials, such as MCM-41 and SBA-15 [34–39].

**Table 1.** Percentage of mass losses and respective temperature ranges for the samples SBA-15 and AISBA-15 (Si/Al = 50) at a heating rate of 10 °C/min.

Mesoporous Material	Temperature Range (°C) and Mass Loss (%)				
	30–130	130–450	450–650	30–650	30–900
SBA-15	2.1	45.2	3.9	51.1	52.2
AISBA-15	12.9	32.8	5.6	51.3	52.7

According to the data in Table 1, it is observed that comparing the total mass loss from 30 to 900 °C for the samples, there is no significant variation (from 52.3 to 52.7%), around 0.5% in mass. The difference in the percentage of mass loss among the materials relative to the first event, the removal of physisorbed water in the pores of the materials, can be attributed to the humidity to which each sample was exposed before thermogravimetric analysis. Thus, the highest percentage of mass loss in the AISBA-15 sample (Si/Al = 50) may be related to physically adsorbed water due to the presence of aluminum and the template removal, which would be explained by the minor mass loss in the second event. The variation in the percentage of mass loss presented in the third event associated with the interstitial water may be an indication that the aluminum incorporated into the synthesis gel of the SBA-15 material interferes with the condensation of the silanol groups. Aluminum can be incorporated into the SBA-15 network both inside the network and on the surface of the material. The greater mass loss due to silanol condensation is evidence that there is more aluminum on the surface of the materials.

It was also observed that by increasing the heating rate from 5 to 10 and 20 °C/min, the temperature shifts to higher values, suggesting a variation in energy in the process for removal of the P123 template from the pores of the materials. Thus, by applying multiple heating rate kinetic models [40–43], the values of the apparent activation energy ( $E_a$ ) for this heat treatment process were in the range of  $E_a = 158$ – $162$  kJ/mol for SBA-15, and from  $E_a = 175$ – $243$  kJ/mol for AISBA-15. The introduction of Al onto the SBA-15 structure suggests that  $Al^{3+}$  ions are present in the hexagonal structure, forming (-Si-O-Al-) interactions typical of aluminosilicate, consequently generating surface acid sites [44–49].

From the TG/DTG data, the temperature of 550 °C was selected for calcination of both materials. After the support calcination process, the active phases of cobalt and molybdenum were deposited on the mesoporous materials SBA-15 and AISBA-15 using the excess solvent co-impregnation method. Thermogravimetry was also used to analyze the decomposition profiles of cobalt nitrate and ammonium heptamolybdate and thus determine the best conditions for calcining the catalysts. Figure 3 shows the TG/DTG curves of the decomposition of the precursor salts of Mo and Co supported on the SBA-15 and AISBA-15 materials. The materials were calcined again in an air atmosphere to decompose the cobalt and molybdenum precursor salts into the respective oxides on the surface of the mesoporous supports and thus obtain the CoMo/SBA-15- and CoMo/AISBA-15-supported catalysts.

From TG/DTG curves (Figure 3), four mass loss events were observed in the following temperature ranges: (i) 30–130 °C, (ii) 130–240 °C, (iii) 240–310 °C, and (iv) 310–410 °C, corresponding to steps for decomposition of the precursor salts inside the mesoporous supports SBA-15 and AISBA-15. The values of mass loss relative to each step of decomposition are provided in Table 2.

From the obtained data, it was observed that up to 450 °C, the salts were completely decomposed on the surface of the materials, and this temperature was taken as a reference for thermal treatment. Thus, the calcination was carried out at this temperature under an air atmosphere flowing at 100 mL/min, in which the Co and Mo salts undergo complete decomposition, generating the CoMo/SBA-15 and CoMo/AISBA-15 HDS catalysts.

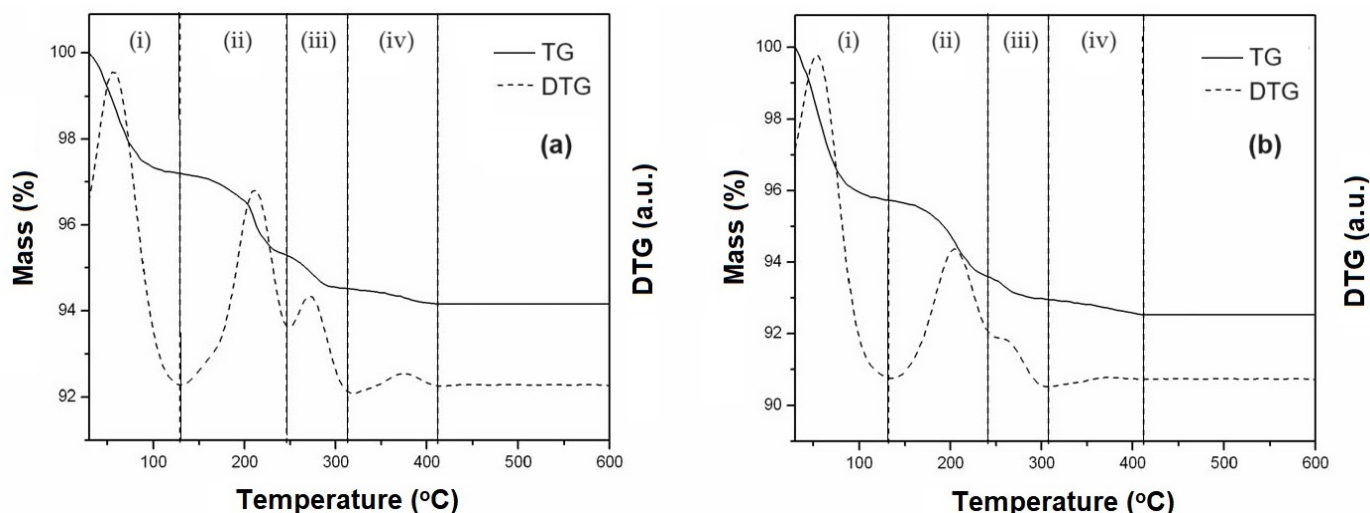


**Figure 3.** Thermogravimetry (TG) and derivative thermogravimetry (DTG) curves, obtained at a heating rate of 10 °C/min, showing the decomposition steps of Co and Mo salts for obtaining the supported mesoporous HDS catalysts: (a) CoMo/SBA-15 and (b) CoMo/AlSBA-15.

**Table 2.** Percentage of mass losses and respective temperature ranges for each step of decomposition of Co and Mo salts for obtaining CoMo/SBA-15 and CoMo/AlSBA-15.

Mesoporous Material	Temperature Range (°C) and Mass Loss (%)				
	(i) 30–130	(ii) 130–240	(iii) 240–310	(iv) 310–410	Total 30–410
CoMo/SBA-15	2.8	1.85	0.82	0.37	5.84
CoMo/AlSBA-15	3.14	2.76	0.95	0.51	7.36

## 2.2. X-ray Diffraction

The X-ray diffractograms (XRDs) of the materials obtained in calcined form were used to identify the hexagonal structure characteristic of mesoporous materials type SBA-15 [50,51]. Emphasis was placed on observing the obtaining of the three main diffraction peaks, referring to the crystalline planes, whose Miller indices are (100), (110), and (200). Two more peaks are observed, whose Miller indices are (210) and (300), indicating excellent textural uniformity of the material [52]. The first three peaks are characteristic of a two-dimensional  $p6mm$  hexagonal symmetry, common to SBA-15-type materials [53,54]. Figure 4a,b show the X-ray diffractograms of mesoporous materials of SBA-15 and AlSBA-15 (Si/Al = 50), respectively.

The XRD analysis of CoMo-supported catalysts was carried out in two steps: low angle (0.5 to 5.0 degrees) and high angle (5.0 to 60.0 degrees), for observation of the ordered hexagonal phase and the presence of CoMo metal oxides, as shown in Figures 5 and 6, for CoMo/SBA-15 and CoMo/AlSBA-15, respectively.

From the diffractograms presented, the presence of the five main diffraction peaks was observed, whose Miller indices are (100), (110), (200), (210), and (300), indicating that high-quality mesoporous materials with defined structure were obtained, with well-ordered hexagonal arrangement [55]. Diffraction peaks for non-supported materials present a better definition in relation to CoMo-supported; this fact is due to the presence of heteroatom on the ordered structures. The mesoporous hexagonal arrangement parameter  $a_0$  (lattice parameter) of the SBA-15 structure is obtained from the reflection peak for the (100) plane, which is the most characteristic in the X-ray diffractogram, whose values are summarized in Table 3.

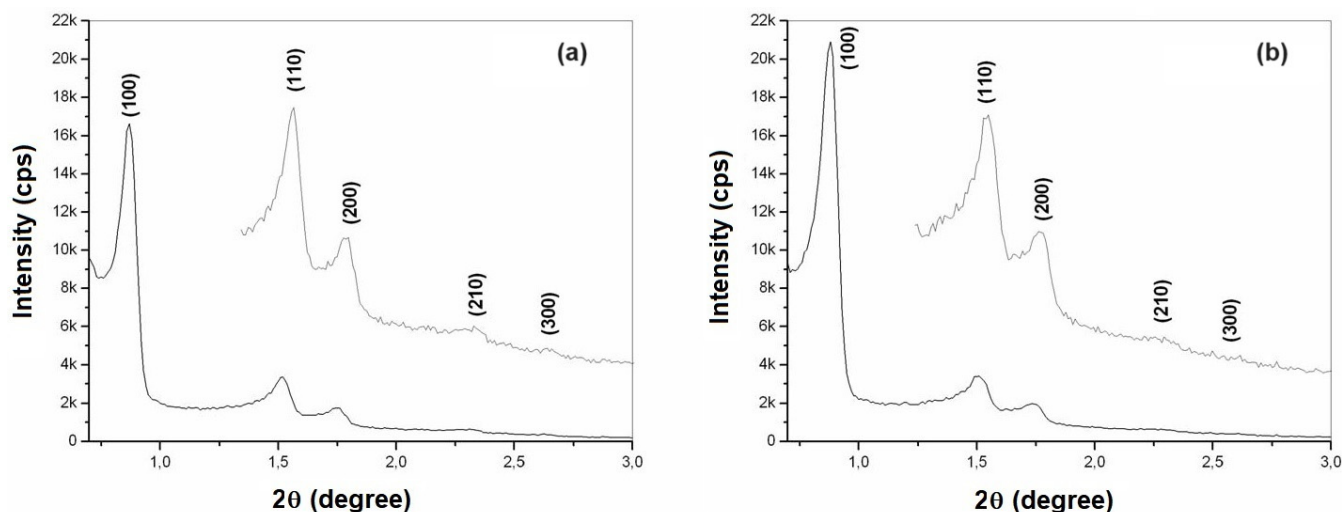


**Figure 4.** X-ray diffractograms of the calcined mesoporous materials: (a) SBA-15 and (b) AISBA-15, showing the Miller indices.

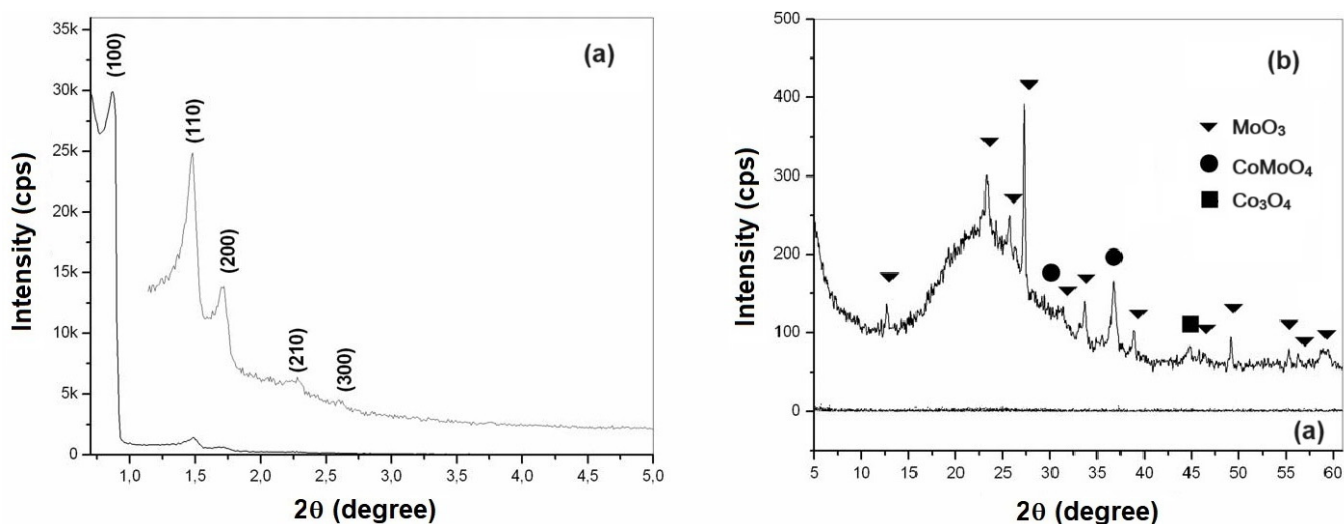


**Figure 5.** X-ray diffractograms of the calcined CoMo/SBA-15 obtained at low (a) and high (b) diffraction angles.

Analyzing the data on the mesoporous parameter ( $a_0$ ) of the SBA-15 and AISBA-15 supports from Table 3, it can be noted that in all cases, there was a decrease in the value of this parameter. That value ( $a_0$ ) represents the sum of the pore diameter ( $d_p$ ) and the silica wall thickness ( $w_t$ ). This decrease may have occurred due to the deposition of nanoparticles of cobalt and molybdenum oxides inside the mesopores of the materials.

The crystalline phases of cobalt and molybdenum oxides were identified through the crystallographic charts of these oxides found in the JCPDS (Joint Committee on Powder Diffraction Standards)/ICDD (International Center for Diffraction Data) library [56]. Research on crystallographic charts verified the presence of  $\text{MoO}_3$  (JCPDS Chart: 05-0508) with an orthorhombic structure,  $\text{Co}_3\text{O}_4$  (JCPDS Chart: 43-1003) with a cubic structure, and mixed oxides of cobalt and molybdenum in the form of  $\text{CoMoO}_4$  (JCPDS Registration: 21-0868) with a monoclinic structure [56]. The main peaks identified based on JCPDS were as follows:  $\text{MoO}_3$  ( $2\theta = 12.79, 23.32, 25.88, 27.32, 33.12, 33.72, 35.46, 38.96, 39.66, 38.96, 39.66, 45.76, 46.3, 49.26, 52.22, 54.13, 55.12, 56.36, 57.59, \text{ and } 58.75$ ),  $\text{CoMoO}_4$  ( $2\theta = 26.40, 28.34, 31.98, \text{ and } 36.63$ ) and  $\text{Co}_3\text{O}_4$  ( $2\theta = 18.93, 31.38, 36.92, 38.52, 44.97, 55.57, \text{ and } 59.49$ ). In all samples studied, the predominance of the crystalline phases  $\text{MoO}_3$  and  $\text{CoMoO}_4$  was observed. The presence of a diffraction peak at 44.97 degrees, corresponding to  $\text{Co}_3\text{O}_4$ , was

identified in all samples. Other cobalt and molybdenum oxides may also have occurred, but in very small quantities not identified from XRD due to interference with background radiation or because they are present in amorphous form.

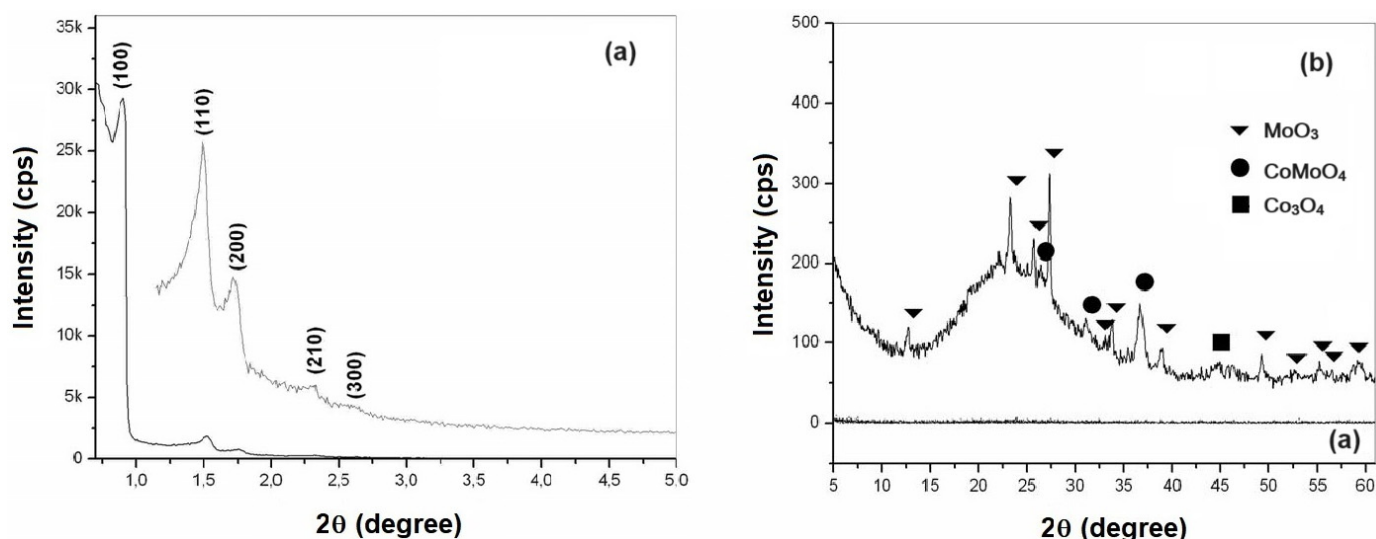


**Figure 6.** X-ray diffractograms of the calcined CoMo/AlSBA-15 obtained at low (a) and high (b) diffraction angles.

**Table 3.** Crystallographic properties of calcined SBA-15, AlSBA-15, CoMo/SBA-15, and CoMo/AlSBA-15 materials.

Materials	(hkl)	2q (°)	d <sub>(hkl)</sub> (nm)	a <sub>o</sub> (nm)
SBA-15	(100)	0.868	10.18	11.76
	(110)	1.516	5.83	
	(200)	1.748	5.05	
	(210)	2.313	3.82	
	(300)	2.630	3.36	
AlSBA-15(Si/Al = 50)	(100)	0.892	9.91	11.44
	(110)	1.503	5.88	
	(200)	1.738	5.08	
	(210)	2.282	3.87	
	(300)	2.610	3.38	
CoMo/SBA-15	(100)	0.873	10.12	11.69
	(110)	1.489	5.94	
	(200)	1.714	5.16	
	(210)	2.275	3.88	
	(300)	2.560	3.45	
CoMo/AlSBA-15(Si/Al = 50)	(100)	0.907	9.74	11.25
	(110)	1.528	5.78	
	(200)	1.733	5.10	
	(210)	2.284	3.87	
	(300)	2.623	3.37	

### 2.3. Nitrogen Adsorption

The adsorption and desorption isotherms, as well as the distribution of pore diameters obtained for samples SBA-15 and AlSBA-15, are presented in Figures 7 and 8, respectively. It can be observed that type IV isotherms were obtained in the samples, according to the IUPAC classification, which is characteristic of mesoporous materials. Accordingly, the hysteresis found was type I, which is characteristic of materials with a cylindrical pore

system or made from aggregates or clusters of spheroidal particles with pores of uniform size [57].

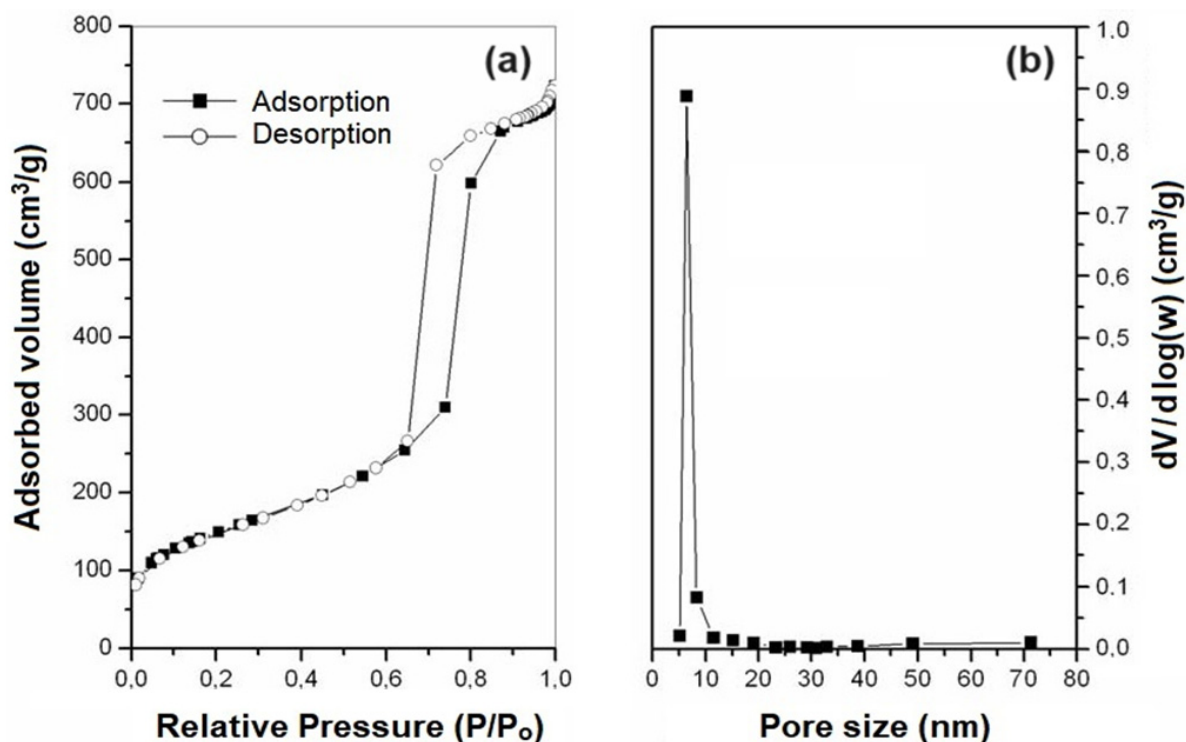


**Figure 7.** (a)  $N_2$  adsorption isotherms and (b) pore size distribution of the SBA-15 mesoporous support.

SBA-15 and AISBA-15 are types of mesoporous materials known for their well-defined pore structures. These materials contain both micropores and mesopores, which contribute to their unique properties and applications. The micropores are primarily formed within the walls of the silica framework, arising from the arrangement of silica units during the synthesis process. They provide additional surface area and can influence the adsorption and diffusion of small molecules and ions. The presence of micropores enhances the overall surface area and adsorption capacity of the material. However, mesopores are the dominant type of pore and are responsible for the ordered and uniform pore structures characteristic of these materials. Mesopores are formed between the silica walls, creating channels or void spaces that allow for the efficient diffusion of molecules within the material. These larger pores enable the transport of larger molecules and facilitate mass transfer processes. The presence of both micropores and mesopores in SBA-15 and AISBA-15 contributes to their high surface area, large pore volume, and uniform pore size distribution. This combination of pore characteristics makes them attractive materials for HDS applications, where precise control over pore structure and surface properties is essential.

The surface areas of the mesoporous materials obtained were determined from data on nitrogen adsorption isotherms at 77 K using the BET model [58] in the  $P/P_0$  range of 0.05–0.20. The pore diameter distributions of mesoporous materials were obtained by the BJH method [59] correlating the desorbed volume values as a function of relative pressure ( $P/P_0$ ) in the algorithms in a pore range of 1–80 nm. The average pore diameters were estimated through the pore distribution curves obtained by the BJH method and revealed values of 6.84 and 6.91 nm for SBA-15 and AISBA-15 (see Table 4), with low variation. After the impregnation of Co and Mo metals, these values decreased to 6.11 and 6.82, respectively. As summarized in Table 4, the obtained materials presented pore volumes in the range of 0.84 to 1.12  $\text{cm}^3/\text{g}$ . Using the BET method, it was observed that the samples had surface

areas in the range of 402 to 602 m<sup>2</sup>/g. These values are compatible with those found in the literature for SBA-15 containing aluminum [60,61].

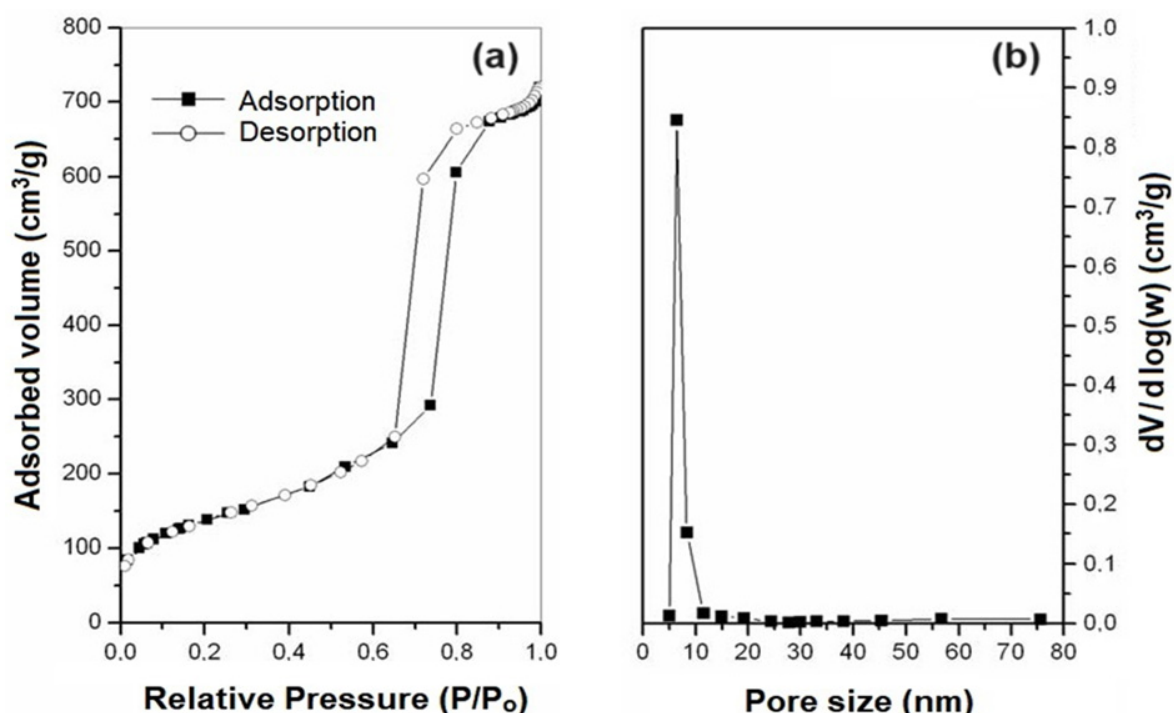


**Figure 8.** (a) N<sub>2</sub> adsorption isotherms and (b) pore size distribution of the AISBA-15 mesoporous support.

**Table 4.** Surface properties of the mesoporous materials, determined from XRD and nitrogen adsorption.

Sample	$a_0$ (nm)	Dp (nm)	Wt (nm) *	Vp (cm <sup>3</sup> g <sup>-1</sup> )	S <sub>BET</sub> (m <sup>2</sup> g <sup>-1</sup> )
SBA-15	11.76	6.84	4.92	1.12	602
AISBA-15	11.44	6.91	4.53	1.07	495
CoMo/SBA-15	11.69	6.11	5.58	0.95	406
CoMo/AISBA-15	11.25	6.82	4.43	0.84	402

$a_0$ : mesoporous parameter; Dp: pore diameter; Wt: wall thickness \* (Wt =  $a_0 - Dp$ ); Vp: pore volume, obtained from the BJH method.

It was observed that there was a decrease in the mesoporous parameter, the sum of the average pore diameter (Dp), and the silica wall thickness (Wt) with the introduction of Al on the support. The average pore diameter did not vary significantly with the introduction of Al. The average values of the silica wall thickness (Wt) can give these materials high mechanical resistance and the possibility for application as catalytic supports in processes of oil refining, where catalysts are often subjected to operating conditions with high temperatures and pressures [62,63]. The structure and pore system of the materials, showing hexagonal ordering with micropores and mesopores, is shown in Figure 9.

The determination of the wall thickness (Wt) of SBA-15 and AISBA-15 mesoporous materials can be achieved through various experimental techniques and characterization methods. Small-angle X-ray diffraction provided structural insights by analyzing the intense peak at an interplanar distance of  $d_{(100)}$ , while nitrogen adsorption–desorption isotherms indirectly inferred the wall thickness (Wt) through BET analysis. The nitrogen physisorption offered additional means to determine pore size distribution and local atomic connectivity, contributing to wall thickness estimation. The combination of these methods is often utilized to comprehensively characterize the structure and properties

of SBA-15 materials, considering factors such as sample preparation requirements and thermal treatments.

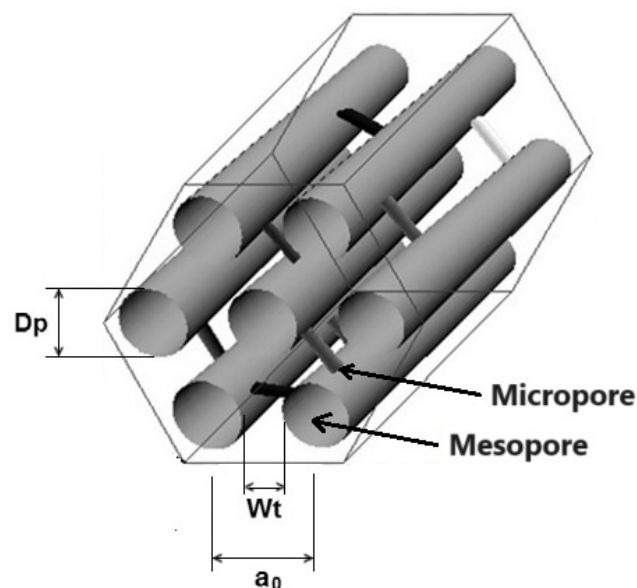


**Figure 9.** Hexagonal arrangement of the mesoporous structure of the SBA-15, showing the mesoporous parameter ( $a_0$ ), wall thickness ( $W_t$ ), and pore size diameter ( $D_p$ ).

After the impregnation of cobalt and molybdenum oxides on the supports, there were no changes in the shapes of the adsorption and desorption isotherms, continuing to be type IV, thus maintaining the mesoporous structure. The average pore diameter decreased with the introduction of Al into SBA-15. With the introduction of Co and Mo metals, the pore volumes were  $0.95$  and  $0.84 \text{ cm}^3 \text{ g}^{-1}$ , and the surface areas were  $406$  and  $402 \text{ m}^2 \text{ g}^{-1}$  for CoMo/SBA-15 and CoMo/AlSBA-15, respectively, and a decrease in the total surface area in relation to the mesopore supports was observed.

#### 2.4. Scanning Electron Microscopy

Scanning Electron Microscopy (SEM) provided surface topography images of the materials, and they were obtained at magnifications of  $15,000\times$  of the SBA-15 and AlSBA-15 materials, as shown in Figure 10. The micrographs of CoMo/SBA-15 and CoMo/AlSBA-15 with details of the pore systems are shown in Figures 10 and 11, respectively. The SEM analyses were carried out with the aim of observing the morphology of the synthesized nanostructured materials. It can be seen in the figures that silica fibers with micrometric dimensions are formed from the linear adhesion of nodules of submicrometric particles. The morphology of the AlSBA-15 (samples with Si/Al = 50) was similar to the SBA-15 sample, even after the impregnation of Co and Mo. In all cases, non-uniform fibers were observed, giving the appearance of “intertwined bead necklaces” [64–66], indicating that this is probably the phase corresponding to SBA-15 since XRD and nitrogen adsorption analyses showed that these samples are pure and have a high degree of ordering and suitable porosity, as shown in Figures 11 and 12.

In hydrodesulfurization reactions,  $\text{MoO}_3$  and  $\text{CoMoO}_4$  species can, during the HDS and sulfidation steps, transform into the  $\text{MoS}_2$  and “CoMoS” phases, which are active and stable for the reaction. The presence of  $\text{Co}_3\text{O}_4$  can give rise to  $\text{Co}_9\text{S}_8$ , a phase that is very inactive for HDS catalysts but can also be reduced to metallic cobalt, which, properly accommodated at the ends of  $\text{MoS}_2$  crystals, gives rise to active phases, known as “CoMoS” [67–69].

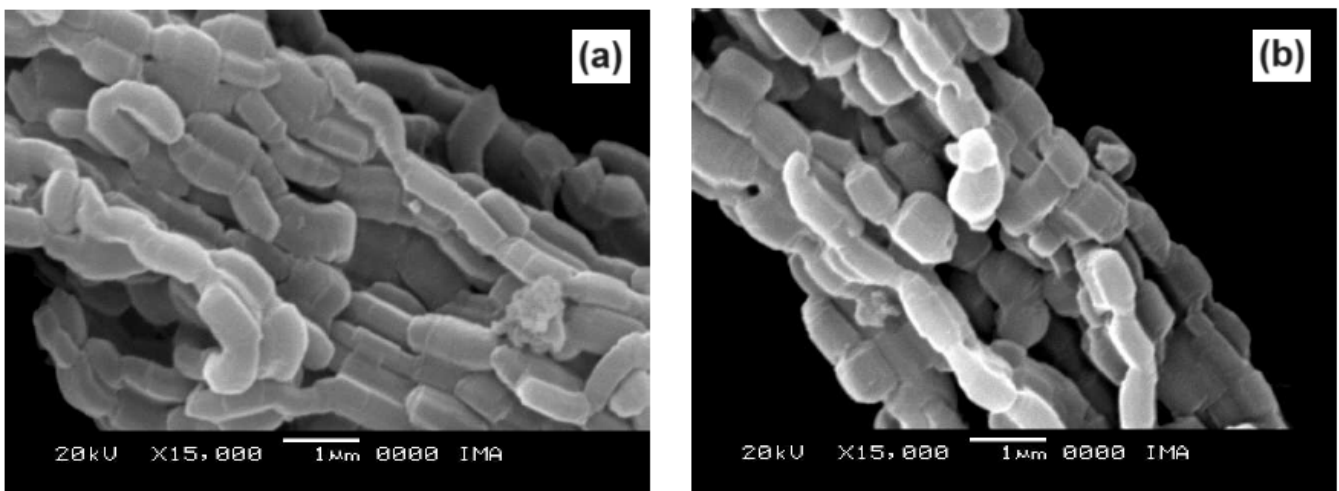


**Figure 10.** Scanning electron micrographs of the mesoporous supports: (a) SBA-15 and (b) AISBA-15 (Si/Al = 50).

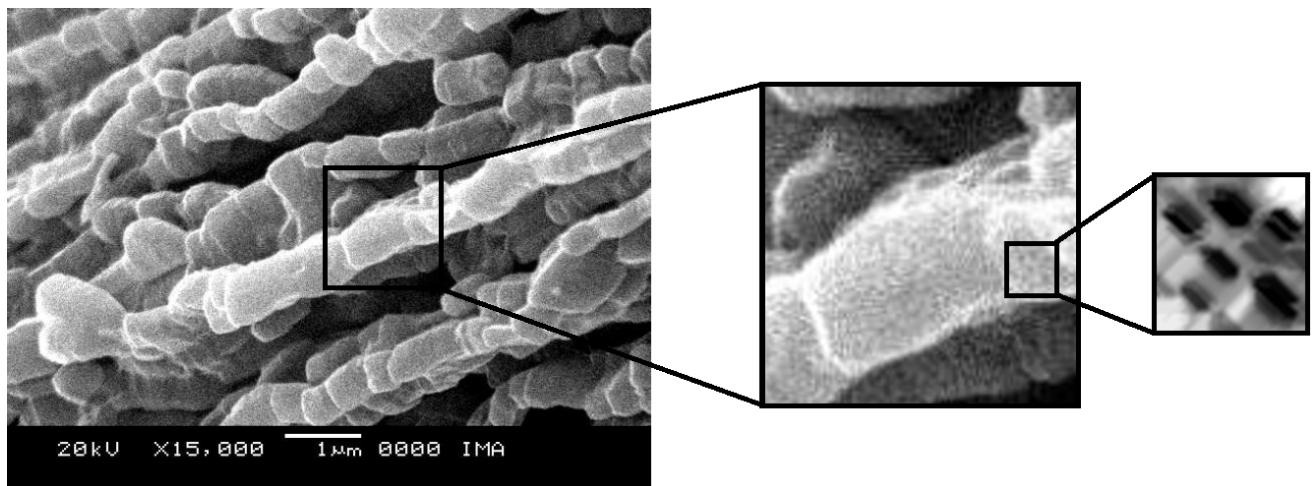


**Figure 11.** Scanning electron micrograph of the mesoporous CoMo/SBA-15 catalyst showing details of porosity.

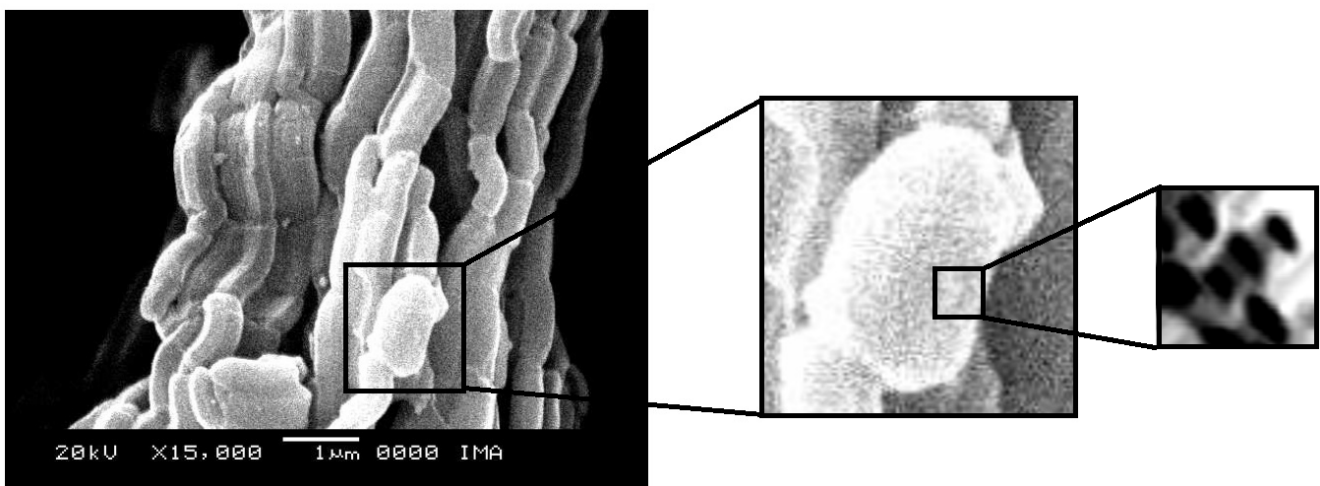


**Figure 12.** Scanning electron micrograph of the mesoporous CoMo/AISBA-15 catalyst showing details of porosity.

### 2.5. Catalytic Activities of CoMo/SBA-15 and CoMo/AlSBA-15

Before starting the catalytic tests for hydrodesulfurization of thiophene, some preliminary tests were carried out with the aim of verifying the occurrence of thermal cracking reactions under the operating conditions of the tests. The first test consisted of a mixture of 13,500 ppm of thiophene (ca. 5100 ppm of sulfur) in n-heptane steam through the reactor at 350 °C without a catalyst, with the aim of observing the occurrence of thermal degradation of the mixture at this temperature, which was not observed, where the chromatogram showed only the peaks relating to thiophene and n-heptane. The second test was conducted to verify the occurrence of catalytic cracking of pure n-heptane on the catalytic bed at 350 °C containing the obtained catalysts. Once again, no peaks other than n-heptane were detected, proving that there was no catalytic cracking under these conditions. After preliminary tests, catalytic hydrodesulfurization tests (HDS) of the mixture of 13,500 ppm of thiophene in n-heptane (ca. 5100 ppm of sulfur) were carried out with the objective of evaluating the conversion and selectivity of 15% CoMo/SBA-15 and 15% CoMo/AlSBA-15 catalysts (Si/Al = 50). According to chromatograms, H<sub>2</sub>S and C<sub>4</sub>-hydrocarbon compounds were typically obtained in the following elution order: isobutane, 1-butene, n-butane, trans-2-butene, and cis-2-butene. The presence of butadiene or isobutene was not observed. In thiophene HDS reactions, butadiene can occur as a primary reaction product or act as an intermediate to obtain butenes through a hydrogenation reaction, thus having a very short lifetime in the catalytic cycle and not appearing in appreciable quantities in product distribution [70]. In the case of isobutene, this product is thermodynamically unfavorable, with the conversion of linear butenes being preferred.

Figure 13a,b show the conversion and paraffin/olefin ratio, respectively, for HDS reactions on catalysts with 15% cobalt and molybdenum metal phase supported on SBA-15, AlSBA-15 (Si/Al = 50). Figure 14a,b show the selectivity for the products. The conversion and selectivity were defined according to Equations (1) and (2), respectively.

$$\text{Conversion(\%)} = \frac{\text{mol(i)Thiophene} - \text{mol(f)Thiophene}}{\text{mol(i)Thiophene}} \quad (1)$$

$$\text{Selectivity to P(\%)} = \frac{\text{mol of Thiophene converted to P}}{\text{mol of Thiophene converted}} \quad (2)$$

where “mol(i)” and “mol(f)” represent the initial and final molar quantities obtained by analyzing the chromatograms at the beginning and end of the reaction, respectively. The letter “P” represents the reaction product measured at the reactor outlet, which may be butane, isobutane, 1-butene, cis-2-butene, or trans-2-butene. The paraffin/olefin ratio was determined considering the selectivity of (n-butane + isobutane) divided by the selectivity of (1-butene + cis-2-butene + trans-2-butene).

It was observed that in the first 15 min of reaction, the highest conversion values were obtained for all catalysts studied. These conversions progressively decreased until reaching stability normally after 60 min of reaction. Considering the conversion values obtained in 120 min of reaction, the CoMo/SBA-15 was more active than the CoMo/AlSBA-15. Also, it was observed that after 60 min of reaction, the paraffin/olefin ratio increased for CoMo/SBA-15, whereas with the CoMo/AlSBA-15, this ratio was almost constant, with values below 0.1. Through X-ray diffraction analyses, no diffractions of amorphous phases of MoO<sub>3</sub> or other diffractions related to Co<sub>3</sub>O<sub>4</sub> were observed other than that found for all samples. According to a previous report [71], cobalt appears as a promoter for the hydrogenolysis reactions of the C-S bonds of thiophene, but it can also act as a promoter for other reactions, such as isomerization and hydrogenation of butadiene after the HDS catalytic cycle. This promoting effect of cobalt can be attributed to the transfer of electrons to molybdenum oxide, reducing its oxidation state from Mo<sup>6+</sup> to Mo<sup>4+</sup>.

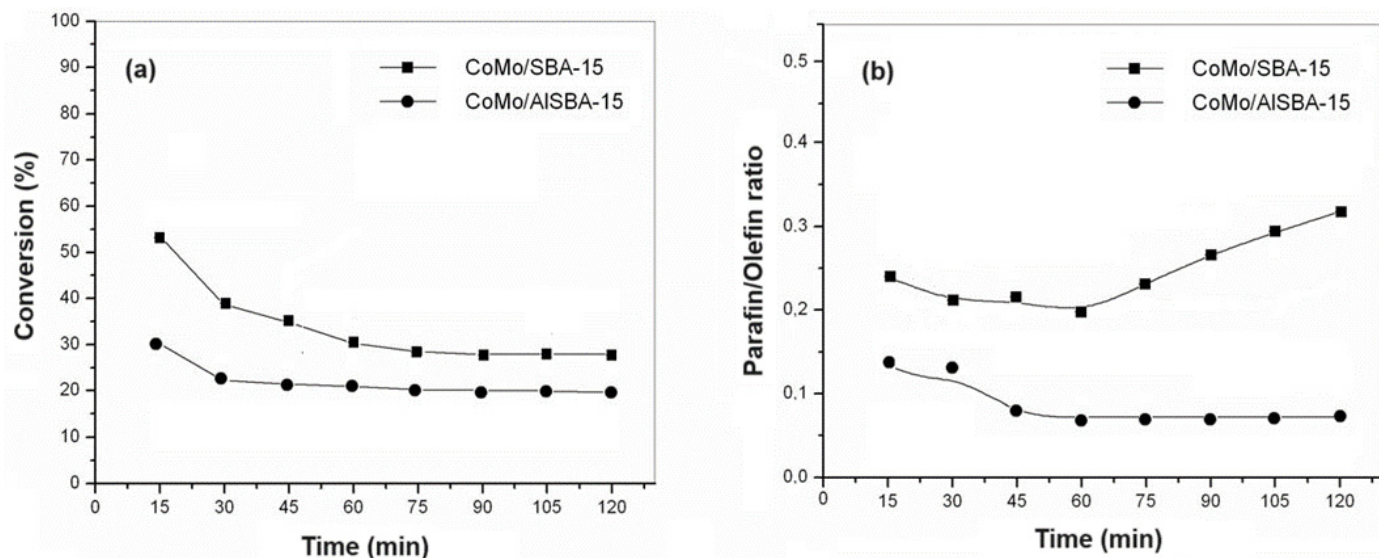


**Figure 13.** Catalytic activity for the CoMo/SBA-15 and CoMo/AISBA-15 catalysts: (a) conversion as a function of reaction time and (b) paraffin/olefin ratio as a function of reaction time.

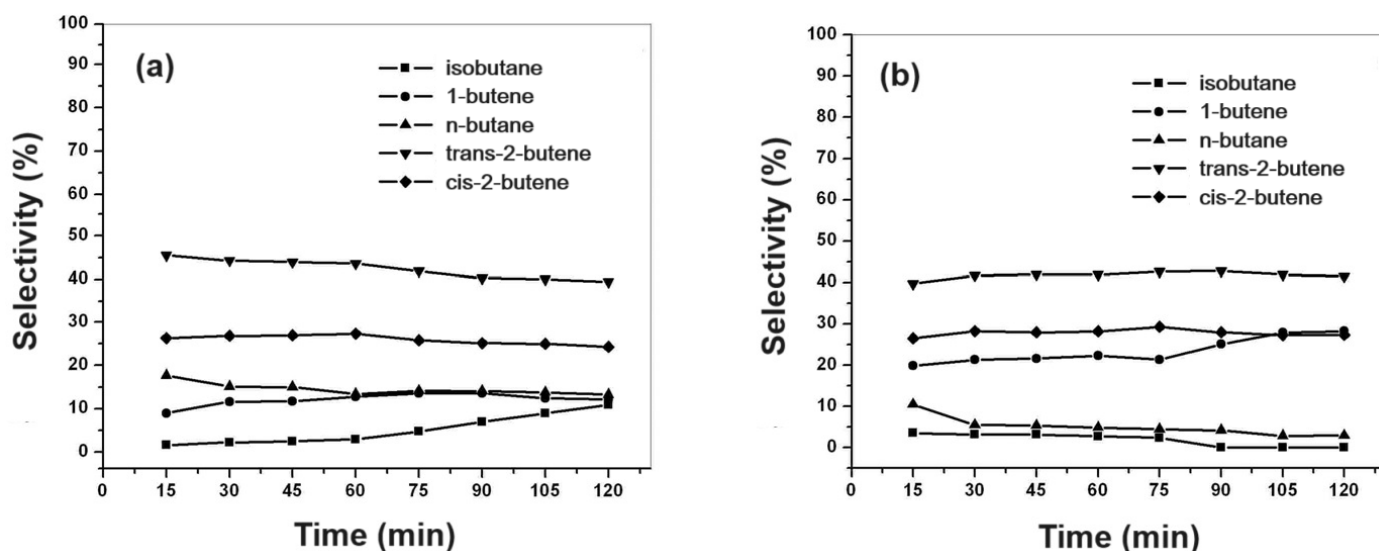


**Figure 14.** Product selectivity to paraffins and olefins as a function of reaction time for the mesoporous catalysts: (a) CoMo/SBA-15 and (b) CoMo/AISBA-15.

A proposed reaction mechanism of thiophene on  $\text{MoO}_3$  considers that the formation of butenes and n-butane can occur directly through one or two butadiene hydrogenation steps, forming 1-butene or n-butane, respectively [3]. Through the isomerization of 1-butene, it is possible to obtain cis-2-butene and trans-2-butene by displacing the double bond. Isobutane can be obtained through chain isomerization of n-butane. The presence of 1,3-butadiene and tetrahydrothiophene (THT) molecules was not detected. Thus, it is supposed that these compounds suffer interconversion reactions inside the mesopores of the CoMo/SBA-15 and CoMo/AISBA-15 catalysts, as schematized in Figure 15.

It is known that some transition metals are effective catalysts for hydrodesulfurization (HDS) reactions, and molybdenum (Mo) and cobalt (Co) are most commonly used. The Co and Mo metals play different roles in the HDS process, and sometimes, the catalysts are composed of combinations of these metals for enhanced performance. In general, Mo facilitates the breaking of carbon-sulfur bonds in sulfur-containing compounds, promoting desulfurization. It has a high affinity for sulfur, enabling it to form stable sulfide compounds on the catalyst surface. Mo also helps in hydrogenation reactions, which are often

coupled with desulfurization in HDS processes. Co-based catalysts are less common than Mo-based catalysts but are still used in certain HDS applications. Co facilitates desulfurization reactions by breaking carbon-sulfur bonds. Co-based catalysts also exhibit suitable selectivity toward thiophene conversion. Catalysts used in industrial HDS processes contain combinations of these metal species, such as Co-Mo, to leverage their synergistic effects. Thus, Mo facilitates the initial breaking of carbon-sulfur bonds, while Co promotes further desulfurization and hydrogenation reactions. Additionally, the presence of mesoporous silica support (SBA-15 or AISBA-15) can enhance the catalyst ability, improving the sulfur removal efficiency.

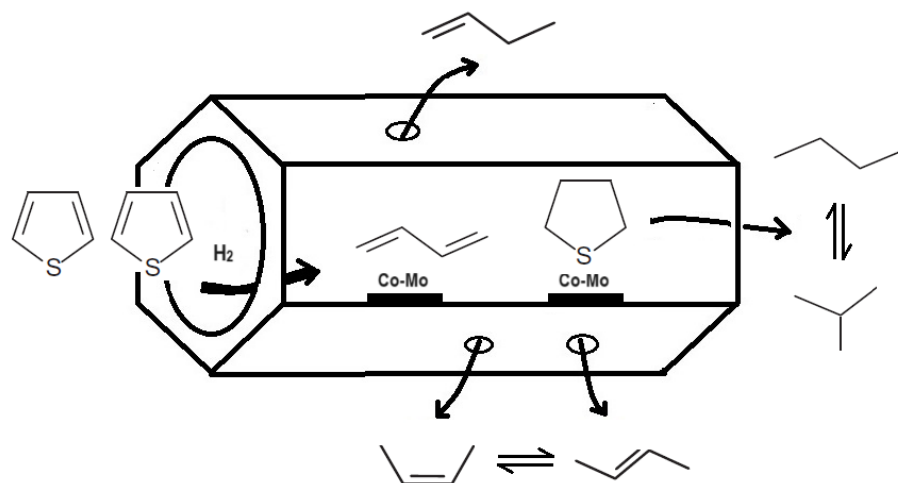


**Figure 15.** Possible HDS thiophene reaction inside the mesopore system of the CoMo/SBA-15 and CoMo/AISBA-15 catalysts and desorption of the products.

According to the obtained results, it was proposed that thiophene molecules suffer desulfurization in the presence of hydrogen to form 1,3-butadiene and hydrogenation to form tetrahydrothiophene (THT). In the presence of Co and Mo metals, 1,3-butadiene reacts with hydrogen to obtain 1-butene and 2-butene, and this suffers isomerization to cis- and trans-2-butene. The THT species are adsorbed on Co-Mo metals, and a new step of desulfurization is suggested for the formation of paraffins, n-butane, and a subsequent isomerization to isobutane. The selectivity for n-butane suggests that it forms via secondary reactions of primary products. Therefore, after one hour of reaction, using the CoMo/SBA-15 catalyst, the isobutane selectivity increased with n-butane decreasing with reaction time, suggesting a step of isomerization.

For the CoMo/AISBA-15 catalyst, this behavior was not observed, indicating that the presence of aluminum, generating Bronsted acid sites, stabilizes the structure and inhibits the paraffin isomerization. From the conversion, selectivity, and paraffin/olefin ratio, a mechanistic scheme for thiophene HDS is proposed in Figure 16, showing a sequence of primary and secondary reactions.

One probable explanation for the presence of acid sites on the CoMo/SBA-15 catalyst can be attributed to silanol groups ( $\equiv\text{Si-O-H}$ ) inside the micropores (Si-OH bulk), with acid character due to the formation of hydrogen bonds, in addition to moderate acidity on the surface of the mesopores (associated Si-OH), forming hydrogen bonds on the external surface of silicon oxide [72]. Another possibility that must be considered is the reactions of H<sub>2</sub>S generated in the HDS reaction, with oxygen from the silicate groups forming sulfated silica with surface proton sites [73]. In this case, we would have the formation of Bronsted super-acidic sites on the internal surface of the mesopores, as proposed in Figure 17, with the sulfated CoMo/SBA-15 catalyst presenting silanol groups capable of donating or accepting hydrogen bonds with different strengths, consequently promoting an increase in the concentration of isobutane from the isomerization process of n-butane.

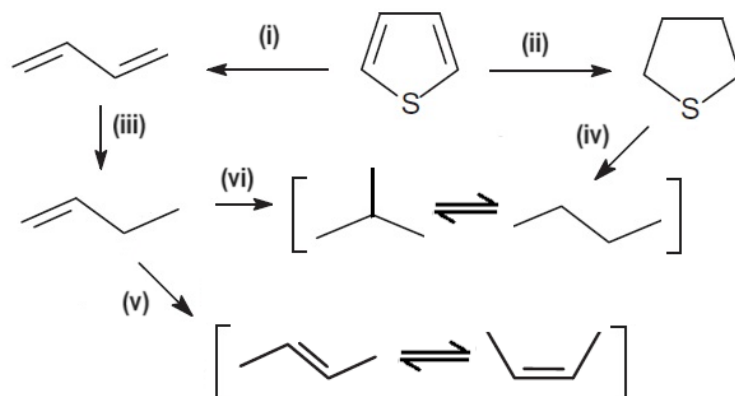


**Figure 16.** Proposed mechanism reaction for hydrodesulfurization of thiophene using the mesoporous CoMo/SBA-15 and CoMo/ALSBA-15 catalysts, showing steps: (i) desulfurization; (ii) hydrogenation; (iii) skeletal hydrogenation; (iv) desulfurization and decyclization; (v) cis- and trans-isomerization; (vi) hydrogenation and C<sub>4</sub>-paraffins isomerization.

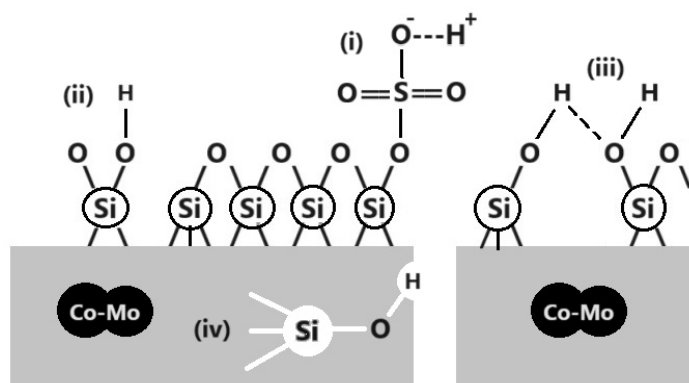


**Figure 17.** Proposed scheme for the silanol groups and acidity on the CoMo/SBA-15 catalyst, evidencing the formation of different hydrogen bonds and acid sites: (i) Bronsted superacid site due to presence of sulfate on the SBA-15 surface; (ii) isolated silanol; (iii) associated silanol; (iv) bulk silanol, showing an acid site on the microporous surface.

### 3. Materials and Methods

#### 3.1. Synthesis of the SBA-15 and ALSBA-15 Supports

The CoMo/SBA-15 and CoMo/ALSBA-15 catalysts were synthesized in two steps: (i) hydrothermal synthesis and calcination of the supports and (ii) impregnation of the Co and Mo on the obtained supports.

The hydrothermal synthesis of mesoporous supports of types SBA-15 and ALSBA-15 with molar ratio Si/Al = 50 were synthesized using the following reagents: tetraethylorthosilicate—TEOS, Sigma-Aldrich, 98%—Si(OC<sub>2</sub>H<sub>5</sub>)<sub>4</sub>, (St. Louis, MO USA), Pseudoboehmite—AlOOH, Vista Chemical Company, 70% Al<sub>2</sub>O<sub>3</sub> and 30% water (Westlake, LA, USA), Pluronic P123 (Triblock Copolymer, BASF Co., average PM = 5750 g/mol, (Houston, TX, USA), hydrochloric acid (Merck, HCl, 37% vol. (Sao Paulo, SP Brazil), and distilled water. The hydrothermal syntheses were carried out using 250 mL Teflon autoclaves wrapped in a stainless steel protection manufactured by Parr Instruments.

The reagents were mixed to obtain a reactive hydrogel with a molar composition of 0.017P123:1.0TEOS:5.7HCl:193H<sub>2</sub>O [74]. First, the P123 template was dissolved in distilled water and HCl, with stirring and heating to 35 °C. Once the temperature was reached, the silica source, tetraethylorthosilicate (TEOS), was added. The mixture was kept under stirring and heated at 35 °C for 24 h (pH = 0–1) to obtain a homogeneous gel. Then, it was transferred to the autoclave and stored in an oven for 48 h, previously heated to 100 °C.

For the AISBA-15 support, the reagents were mixed to obtain a reactive hydrogel with the following molar composition: 0.017P123:1.0 TEOS: $x$ Al<sub>2</sub>O<sub>3</sub>:5.7HCl:193H<sub>2</sub>O. The value of " $x$ " was used to maintain the molar ratio Si/Al = 50.

Once the hydrothermal syntheses were completed, the materials obtained were vacuum filtered and washed with 50 mL of a 2% solution by volume of hydrochloric acid in ethanol. This procedure facilitates the removal of the organic director from the pores of the material, reducing calcination time. After this procedure, each material was placed to dry at room temperature for 24 h. To completely remove P123 from the pores of the mesoporous molecular sieves, the calcination technique was used. In this procedure, each sample was subjected to heating from room temperature to 500 °C under a dynamic nitrogen atmosphere with a flow of 100 mL min<sup>-1</sup> and a heating rate of 10 °C min<sup>-1</sup>. Upon reaching 500 °C, each material remained for one hour under nitrogen in the same flow. After this time, the gas was changed to synthetic air (reactive gas) and heated at the sample temperature for another hour with a flow of 100 mL min<sup>-1</sup>. The supports were called SBA-15 and AISBA-15.

### 3.2. Preparation of the CoMo/SBA-15 and CoMo/AISBA-15

Co and Mo metals were deposited on mesoporous supports using the impregnation technique with excess solvent using absolute ethanol: C<sub>2</sub>H<sub>5</sub>OH (99.5%, Merck, Sao Paulo, SP, Brazil) as solvent, cobalt nitrate hexahydrate: Co(NO<sub>3</sub>)<sub>2</sub>·6H<sub>2</sub>O (99%, Merck, Sao Paulo, SP, Brazil) as a source of cobalt, and ammonium heptamolybdate tetrahydrate: (NH<sub>4</sub>)<sub>6</sub>Mo<sub>7</sub>O<sub>24</sub>·4H<sub>2</sub>O (Ecibra, 82.5% in MoO<sub>3</sub>, Santo Amaro, SP, Brazil) as a source of molybdenum. Before impregnation, all mesoporous supports were subjected to a TG run in a nitrogen atmosphere at a heating rate of 20 °C min<sup>-1</sup> from 30 to 900 °C, with the aim of determining the relative humidity levels of each support, starting from mass losses in the range of 30 to 130 °C, and using these data to correct the dry mass of the supports in order to minimize weighing errors during the deposition stage of the cobalt and molybdenum precursor salts.

The metal impregnation procedure consisted of weighing ca. 0.5 g of the support (SBA-15 or AISBA-15), considering the relative humidity. The amounts of cobalt nitrate, Co(NO<sub>3</sub>)<sub>2</sub>·6H<sub>2</sub>O, and ammonium heptamolybdate, (NH<sub>4</sub>)<sub>6</sub>Mo<sub>7</sub>O<sub>24</sub>·4H<sub>2</sub>O, were weighed in a porcelain crucible and solubilized in 20 mL of absolute ethanol using a glass rod. After the solubilization of the salts, the support was slowly added, stirring with the glass rod. The crucible with the suspension was transferred to the heating mantle at 70 °C, homogenizing periodically to evaporate the excess solvent. After evaporation of the excess ethanol, the crucible was transferred to the oven and dried at 100 °C for 6 h. The depositions of the metallic phases were carried out to obtain a loading of 15% by weight of the active phase, with a [Co/(Co + Mo)] atomic ratio of 0.45.

The synthesis process allows the cobalt and molybdenum ions from the solution to be absorbed into the pores of the support material. After impregnation, the solvent was evaporated, leaving behind the metals distributed on the surface and within the pores of the support materials. The impregnated materials were dried to remove any remaining moisture. The dried catalysts were subjected to calcination at 500 °C under an atmosphere of air flowing at 100 mL/min. This step serves to decompose the cobalt and molybdenum salts and convert them into cobalt and molybdenum oxides on the support material. Finally, before the catalytic evaluation, the calcined materials were subjected to a reduction step in a hydrogen atmosphere. This reduces the cobalt and molybdenum species to their metallic form, the active metal phase required for catalysis.

### 3.3. Physicochemical Characterization of the Obtained Materials

#### 3.3.1. Thermogravimetry (TG)

Thermal analysis using TG was used to carry out studies to determine the best calcination conditions for eliminating P123 from the pores of mesoporous materials SBA-15 and AISBA-15, as well as verifying the best calcination conditions for the decomposition

of the precursor salts of the metallic phases of cobalt and molybdenum. Thermogravimetric analyses of the as-synthesized mesoporous materials (SBA-15 and AISBA-15) were obtained in a thermobalance with a horizontal furnace model TA/SDTA 951 from Mettler (Switzerland, GmbH). The thermogravimetric curves of the non-calcined samples were obtained by heating the sample from room temperature to 900 °C in a dynamic nitrogen atmosphere at three heating rates of 5, 10, and 20 °C min<sup>-1</sup>, with the aim of carrying out a series of kinetic studies regarding the best conditions for removing the P123 template from the pores of the materials and thus establishing the best calcination conditions. For each test, alumina crucibles with a mass of around 10 mg were used.

By using TG, it was possible to study the best conditions for calcining mesoporous materials impregnated with cobalt and molybdenum salts. In all cases, approximately 10 mg of each non-calcined sample was heated from room temperature to 900 °C at a heating rate of 10 °C min<sup>-1</sup>. The curves were obtained in a dynamic synthetic air atmosphere of 25 mL min<sup>-1</sup>.

### 3.3.2. X-ray Diffraction (XRD)

XRD analyses using the powder method were carried out on materials obtained in calcined form, with the aim of verifying whether the mesoporous hexagonal structure had formed. In the samples impregnated after the calcination process, new XRD analyses were carried out to verify variations in the hexagonal mesoporous structure and to identify the crystalline phases of the cobalt and molybdenum oxides formed.

The X-ray diffractograms of the SBA-15 and AISBA-15 samples were obtained in an angular scan of 0.5 to 5.0 degrees on Shimadzu model XRD 6000 equipment (Nakagyo-ku, Kyoto, Japan). The tests were conducted using CuK $\alpha$  radiation and a nickel filter with a tube voltage of 30 kV and a current of 30 mA. The slit had an opening of 0.15 degrees, and the X-ray beam was phased in relation to the sample with a speed of 0.5 degrees/min and a step of 0.01 degrees. For samples containing deposited cobalt and molybdenum oxides, XRD was carried out in an angular range of 5 to 60 degrees.

### 3.3.3. Nitrogen Adsorption

The specific surface area, determined by the BET method, total pore volume, distribution, and average pore size diameter, was determined through N<sub>2</sub> adsorption at the temperature of liquid N<sub>2</sub> (77 K). The experiments of the adsorption isotherms of the calcined samples were carried out on Micromeritics ASAP2010 equipment (Norcross, GA, USA). To this end, approximately 100 mg of each sample was previously treated at 170 °C for 12 h under vacuum and then subjected to nitrogen adsorption at 77 K. The adsorption and desorption isotherms were obtained in a relative pressure ( $P/P_0$ ) range of 0.01 to 0.95. The data relating to the volume of adsorbed gas as a function of partial pressure were correlated using mathematical models to determine the BET surface area [58] and BJH to volume and distribution of pores [59].

### 3.3.4. Scanning Electron Microscopy (SEM)

Scanning electron micrographs of the mesoporous supports SBA-15 and AISBA-15 with Si/Al = 50, as well as the supported cobalt and molybdenum catalysts, were carried out with the aim of observing the morphology of the synthesized mesoporous materials and some change in the morphology after impregnation of the CoMo metals. The analysis was obtained using a Jeol equipment model JSM-5610 LV (Miami, MA, USA). Before analysis, the samples were adhered to the sample holder using a thin carbon tape and subjected to a pretreatment that consisted of the deposition of a thin nanolayer of gold, with the aim of making the sample a suitable electron conductor and thus be able to provide suitable quality and resolution of the images. The analyses were carried out with magnifications ranging from 100 to 25,000 times.

### 3.4. Thiophene Hydrodesulfurization (HDS)

The thiophene HDS catalytic tests were carried out in a fixed-bed continuous-flow reactor under atmospheric pressure, according to the scheme shown in Figure 18. Thiophene was chosen as a probe molecule, which is characterized as the most common sulfur contaminant present in middle petroleum distillates. To carry out the tests, approximately 50 mg of sample was introduced into the Pyrex glass “U” reactor heated from room temperature to 450 °C at a heating rate of 5 °C min<sup>-1</sup> in a dynamic atmosphere of N<sub>2</sub> containing 10% of H<sub>2</sub> with a total flow of 30 mL min<sup>-1</sup>. After reaching 450 °C, the sample remained under these conditions for another 1 h and was then cooled to the reaction temperature of 350 °C, still maintaining the reducing atmosphere. Then, a mixture of n-heptane containing 12,070 ppm of thiophene (ca. 5100 ppm of sulfur) was drawn from a saturator maintained at room temperature through a line heated at 120 °C to the catalytic bed with a flow of 30 mL min<sup>-1</sup>, maintaining the molar ratio H<sub>2</sub>/(thiophene and n-heptane) of 8.2. The composition of the standard mixture of thiophene in n-heptane was confirmed through chemical analysis using EDX-700 equipment Shimadzu (Nakagyo-ku, Kyoto, Japan).

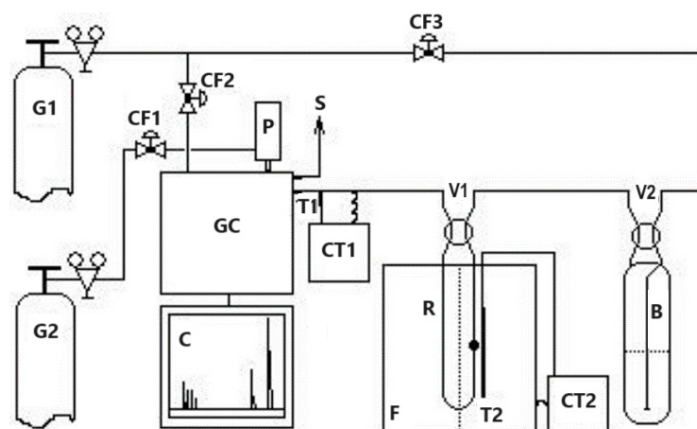


**Figure 18.** Catalytic evaluation unit. Where G1 = hydrogen; G2 = nitrogen; V1, V2, = 4-way valves; CF1, CF2, CF3 = flow control valves; B = saturator; P = 10-way pneumatic valve; CT1, CT2 = temperature controllers; T1, T2 = thermocouples; S = gas output; C = chromatogram; GC = gas chromatograph; F = furnace; and R = reactor with catalyst.

During the reaction, the catalytic bed was maintained at a constant temperature of 350 °C using a COEL HW1500 temperature controller (Sao Paulo, SP, Brazil). The reactor effluent products were successively injected “on-line” through a ten-way valve into a Varian CP3800 gas chromatograph (Palo Alto, CA, USA) with a thermal conductivity detector at 15 min intervals until reaching the pseudo-stationary state. The products were separated and analyzed in a 60 m fused silica column. The identification of products was carried out by comparing the retention times of the analytes of each chromatogram with the retention times of thiophene, n-heptane, and natural gas standards, considering the elution orders of the substances through the stationary phase used in the column (separation based on boiling points) as proposed by the manufacturer. Quantification of chromatogram peaks was performed using the method of external standards analyzed in the linearity range of the detector as recommended for thermal conductivity detectors. The tests were conducted with all catalysts in powder form to minimize the effects arising from internal mass transport. The following aspects were also taken into consideration: isothermal reaction in a fixed bed, vapor phase in an ideal gas state, uniform porosity, and negligible pressure drop in the bed without the presence of axial dispersion effects.

## 4. Conclusions

The effect of mesoporous supports such as silica (SBA-15) and aluminosilicate (AISBA-15) on the catalytic activities of cobalt and molybdenum (CoMo) catalysts was demonstrated

for thiophene hydrodesulfurization in a n-heptane stream as a model reaction. The characterization of the mesoporous supports by nitrogen adsorption–desorption analysis showed that SBA-15 and AISBA-15 (Si/Al = 50) materials possessed surface area, pore diameter, and pore volume appropriate for the impregnation and dispersion of the Co and Mo metals on the surface. The crystallization properties by X-ray diffraction analysis showed that the Co and Mo metals were well dispersed in the catalytic supports. The catalytic activities indicated that the ordering and open pore channel of the CoMo/SBA-15 and CoMo/AISBA-15 mesoporous catalysts are appropriate for thiophene conversion and selectivity to paraffin butane and olefins 1-butene, cis-, and trans-2-butene. The 1,3-butene and tetrahydrothiophene (THT) molecules were not detected in the products, evidencing that these compounds are strongly adsorbed on the Co-Mo active sites and undergo hydrogenation and desulfurization, respectively, with subsequent formation of C<sub>4</sub>-paraffins, such as n-butane and isobutane.

The catalytic activity of CoMo/SBA-15 for thiophene HDS reaction was higher than that of CoMo/AISBA-15, reaching ca. 20 and 30% conversion, respectively, after 1 h of reaction. The same trend was observed for the paraffin/olefin ratio. Therefore, using the CoMo/SBA-15 catalyst, after 1 h of reaction, the paraffin/olefin ratio increased from 0.2 to 0.3 up to 2 h of reaction. With the CoMo/AISBA-15 catalyst, it was found that this ratio remained constant between 1 and 2 h of reaction, with a value lower than 0.1, showing that the AISBA-15 support stabilized the structure. Regarding product selectivity, in general, the two catalysts were selective for the olefins 1-butene and trans- and cis-2-butenes. In relation to paraffins, for the CoMo/SBA-15 catalyst, ca. 10% selectivity was obtained for isobutane and n-butane. On the other hand, using the CoMo/AISBA-15 catalyst, low concentrations of paraffins were observed, with a subsequent increase in the concentration of 1-butene, showing that the n-butane dehydrogenation reaction caused by metallic sites probably occurred, as well as isomerization to iso-butane, due to the presence of Bronsted acid sites generated by Al in the CoMo/AISBA-15 catalyst.

**Author Contributions:** Conceptualization, A.C.S.L.S.C. and J.M.F.B.; methodology, A.C.S.L.S.C. and M.J.B.S.; formal analysis, M.D.S.A. and J.B.S.; investigation and data curation, A.C.S.L.S.C.; data curation, writing—original draft preparation, A.S.A. and R.C.O.B.D.; writing—review and editing, M.D.S.A., A.S.A. and J.B.S.; project administration, A.S.A. and V.J.F.J.; funding acquisition, A.S.A. All authors have read and agreed to the published version of the manuscript.

**Funding:** This research was funded by CNPq, grant number 312461/2022-4.

**Data Availability Statement:** Data are contained within the article.

**Acknowledgments:** The authors thank the Brazilian Agency of Petroleum, Natural Gas and Biofuel (ANP) and the National Council for Scientific and Technological Development (CNPq Brazil) for supporting this research.

**Conflicts of Interest:** The authors declare no conflicts of interest.

## References

1. Ohtsuka, T. Catalyst for hydrodesulfurization of petroleum residua. *Catal. Rev. Sci. Eng.* **1997**, *16*, 291–325. [[CrossRef](#)]
2. Delmon, B.; Li, Y.W. Modeling of hydrotreating catalysts based on the remote control: HYD e HDS. *J. Mol. Catal. A Chem.* **1997**, *127*, 163–190.
3. Topsoe, H.; Clausen, B.S. Importance of Co-Mo type structures in hydrodesulfurization. *Catal. Rev. Sci. Eng.* **1984**, *26*, 395–420. [[CrossRef](#)]
4. Topsoe, H. Characterization of the structures and active sites in sulfided Co-Mo/Al<sub>2</sub>O<sub>3</sub> and Ni-Mo/Al<sub>2</sub>O<sub>3</sub> catalysts by NO chemisorption. *J. Catal.* **1983**, *84*, 386–401. [[CrossRef](#)]
5. Grande, P.; Vanhaeren, X. Hydrotreating catalysts, an old story with new challenges. *Catal. Today* **1997**, *36*, 375–391. [[CrossRef](#)]
6. Morais, C.G.D.P.; Silva, J.B.; Almeida, J.S.; Oliveira, R.R.; Araujo, M.D.S.; Fernandes, G.J.T.; Delgado, R.C.O.B.; Coriolano, A.C.F.; Fernandes, V.J., Jr.; Araujo, A.S. Catalytic Distillation of Atmospheric Residue of Petroleum over HY-MCM-41 Micro-Mesoporous Materials. *Catalysts* **2023**, *13*, 296. [[CrossRef](#)]
7. Yue, L.; Li, G.; Zhang, F.; Chen, L.; Li, X.; Huang, X. Size-dependent activity of unsupported Co–Mo sulfide catalysts for the hydrodesulfurization of dibenzothiophene. *Appl. Catal. A Gen.* **2016**, *512*, 85–92. [[CrossRef](#)]

8. Zepeda, T.A.; de Leon, J.N.D.; Alonso, G.; Infantes-Molina, A.; Galindo-Ortega, Y.I.; Huirache-Acuna, R.; Fuentes, S. Hydrodesulfurization activity of Ni-containing unsupported Ga(x)WS<sub>2</sub> catalysts. *Catal. Commun.* **2019**, *130*, 105760. [[CrossRef](#)]
9. Morales-Ortuno, J.C.; Ortega-Domínguez, R.A.; Hernandez-Hipolito, P.; Bokhimi, X.; Klimova, T.E. HDS performance of NiMo catalysts supported on nanostructured materials containing titania. *Catal. Today* **2016**, *271*, 127–139. [[CrossRef](#)]
10. Shang, H.; Liu, C.; Xu, Y.; Qiu, J.; Wei, F. States of carbon nanotube supported Mo based HDS catalysts. *Fuel Process. Technol.* **2007**, *88*, 117–123. [[CrossRef](#)]
11. Liu, Z.; Zhang, L.; Jiang, J.; Bian, C.; Zhang, Z.; Gao, Z. Advancement of hydrodesulfurization catalyst and discussion of its application in coal tar. *Adv. Chem. Eng.* **2013**, *3*, 36–46. [[CrossRef](#)]
12. Umar, M.; Abdulazeez, I.; Tanimu, A.; Ganiyu, S.A.; Alhooshani, K. Modification of ZSM-5 mesoporosity and application a catalyst support in hydrodesulfurization of dibenzothiophene: Experimental and DFT studies. *J. Environ. Chem. Eng.* **2021**, *9*, 106738. [[CrossRef](#)]
13. Yu, Q.; Zhang, L.; Guo, R.; Sun, J.; Fu, W.; Tang, T.; Tang, T. Catalytic performance of CoMo catalysts supported on meso rous ZSM-5 zeolite-alumina composites in the hydrodesulfurization of 4,6-dimethyldibenzothiophene. *Fuel Process. Technol.* **2017**, *159*, 76–87. [[CrossRef](#)]
14. Qi, L.; Zheng, P.; Zhao, Z.; Duan, A.; Xu, C.; Wang, X. Insights into the intrinsic kinetics for efficient hydrodesulfurization of 4,6-dimethyldibenzothiophene over mesoporous CoMoS<sub>2</sub>/ZSM-5. *J. Catal.* **2022**, *408*, 279–293. [[CrossRef](#)]
15. Zhou, W.; Zhou, A.; Zhang, Y.; Zhang, C.; Chen, Z.; Liu, L.; Zhou, Y.; Wei, Q.; Tao, X. Hydrodesulfurization of 4,6-dimethyldibenzothiophene over NiMo supported on Ga-modified Y zeolites catalysts. *J. Catal.* **2019**, *374*, 345–359. [[CrossRef](#)]
16. Song, H.; Wang, J.; Wang, Z.; Song, H.; Li, F.; Jin, Z. Effect of titanium content on dibenzothiophene HDS performance over Ni<sub>2</sub>P/Ti-MCM-41 catalyst. *J. Catal.* **2014**, *311*, 257–265. [[CrossRef](#)]
17. Souza, M.J.B.; Marinkovic, B.A.; Jardim, P.M.; Araujo, A.S.; Pedrosa, A.M.G.; Souza, R.R. HDS of thiophene over CoMo/AlMCM-41 with different Si/Al ratios. *Appl. Catal. A Gen.* **2007**, *316*, 212–218. [[CrossRef](#)]
18. Calderon-Magdalenos, M.A.; Mendoza-Nieto, J.A.; Klimova, T.E. Effect of the amount of citric acid used in the preparation of NiMo/SBA-15 catalysts on their performance in HDS of dibenzothiophene-type compounds. *Catal. Today* **2014**, *220*, 78–88. [[CrossRef](#)]
19. Soni, K.K.; Chandra Mouli, K.; Dalai, A.K.; Adjaye, J. Effect of Ti loading on the HDS and HDN activity of KLGO on NiMo/TiSBA-15 catalysts. *Microp. Mesop. Mater.* **2012**, *152*, 224–234. [[CrossRef](#)]
20. Alonso-Perez, M.O.; Pawelec, B.; Zepeda, T.A.; Alonso-Núñez, G.; Nava, R.; Navarro, R.M.; Huirache-Acuna, R. Effect of the titanium incorporation method on the morphology and HDS activity of supported ternary Ni–Mo–W/SBA-16 catalysts. *Microp. Mesop. Mater.* **2021**, *312*, 110779. [[CrossRef](#)]
21. Dominguez Garcia, E.; Chen, J.; Oliviero, E.; Oliviero, L.; Mauge, F. New insight into the support effect on HDS catalysts: Evidence for the role of Mo-support interaction on the MoS<sub>2</sub> slab morphology. *Appl. Catal. B Environ.* **2020**, *260*, 117975. [[CrossRef](#)]
22. Roy, T.; Rousseau, J.; Daudin, A.; Pirngruber, G.; Lebeau, B.; Blin, J.-L.; Brunet, S. Deep hydrodesulfurization of 4,6-dimethyldibenzothiophene over CoMoS/TiO<sub>2</sub> catalysts: Impact of the TiO<sub>2</sub> treatment. *Catal. Today* **2021**, *377*, 17–25. [[CrossRef](#)]
23. Mazurelle, J.; Lamonier, C.; Lancelot, C.; Payen, E.; Pichon, C.; Guillaume, D. Use of the cobalt salt of the heteropolyanion [Co<sub>2</sub>Mo<sub>10</sub>O<sub>38</sub>H<sub>4</sub>]<sub>6</sub> for the preparation of CoMo HDS catalysts supported on Al<sub>2</sub>O<sub>3</sub>, TiO<sub>2</sub> and ZrO<sub>2</sub>. *Catal. Today* **2008**, *130*, 41–49. [[CrossRef](#)]
24. Zhang, L.; Chen, Z.; Zheng, S.; Cai, G.; Fu, W.; Tang, T.; He, M. Effect of the Co/Mo Ratio on the Morphology and Activity of the CoMo Catalyst Supported on MgO Nanosheets in Dibenzothiophene Hydrodesulfurization. *Ind. Eng. Chem. Res.* **2020**, *59*, 12338–12351. [[CrossRef](#)]
25. Bing, L.C.; Tian, A.X.; Li, J.J.; Yi, K.F.; Wang, F.; Wu, C.Z.; Wang, G.J. The effects of chelating agents on CoMo/TiO<sub>2</sub>-Al<sub>2</sub>O<sub>3</sub> hydrodesulfurization catalysts. *Catal. Lett.* **2018**, *148*, 1309–1314. [[CrossRef](#)]
26. Li, G.; Li, W.; Zhang, M.; Tao, K. Characterization and catalytic application of homogeneous nano-composite oxides ZrO<sub>2</sub>-Al<sub>2</sub>O<sub>3</sub>. *Catal. Today* **2004**, *93*, 595–601. [[CrossRef](#)]
27. Tavizon Pozos, J.A.; Esquivel, G.C.; Cervantes Arista, I.; de los Reyes Heredia, J.A.; Suarez Toriello, V.A. Co-processing of hydrodeoxygenation and hydrodesulfurization of phenol and dibenzothiophene with NiMo/Al<sub>2</sub>O<sub>3</sub>-ZrO<sub>2</sub> and NiMo/TiO<sub>2</sub>-ZrO<sub>2</sub> catalysts. *Int. J. Chem. React. Eng.* **2022**, *20*, 47–60. [[CrossRef](#)]
28. Kazakov, M.O.; Kazakova, M.A.; Vatutina, Y.V.; Larina, T.V.; Chesalov, Y.A.; Gerasimov, E.Y.; Prosvirin, I.P.; Klimov, O.V.; Noskov, A.S. Comparative study of MWCNT and alumina supported CoMo hydrotreating catalysts prepared with citric acid as chelating agent. *Catal. Today* **2020**, *357*, 221–230. [[CrossRef](#)]
29. Saleh, T.A. Carbon nanotube-incorporated alumina as a support for MoNi catalysts for the efficient hydrodesulfurization of thiophenes. *Chem. Eng. J.* **2021**, *404*, 126987. [[CrossRef](#)]
30. Saleh, T.A.; Al-Hammadi, S.A.; Abdullahi, I.M.; Mustageem, M. Synthesis of molybdenum cobalt nanocatalysts supported on carbon for hydrodesulfurization of liquid fuels. *J. Mol. Liq.* **2018**, *272*, 715–721. [[CrossRef](#)]
31. Prajapati, Y.N.; Verma, N. Hydrodesulfurization of thiophene on activated carbon fiber supported NiMo catalysts. *Energy Fuel* **2018**, *32*, 2183–2196. [[CrossRef](#)]
32. Abubakar, U.C.; Alhooshani, K.R.; Adamu, S.; Al Thagfi, J.; Saleh, T.A. The effect of calcination temperature on the activity of hydrodesulfurization catalysts supported on mesoporous activated carbon. *J. Clean. Prod.* **2019**, *211*, 1567–1575. [[CrossRef](#)]

33. Ali, I.; Al-Arfaj, A.A.; Saleh, T.A. Carbon nanofiber-doped zeolite as support formolybdenum based catalysts for enhanced hydrodesulfurization of dibenzothiophene. *J. Mol. Liq.* **2020**, *304*, 112376. [CrossRef]
34. Araujo, A.S.; Quintella, S.A.; Coutinho, A.C.S.L.S. Synthesis monitoring of SBA-15 nanostructured materials. *Adsorption* **2009**, *15*, 306–311. [CrossRef]
35. Antochshuk, V.; Araujo, A.S.; Jaroniec, M. Functionalized MCM-41 and CeMCM-41 materials synthesized via interfacial reactions. *J. Phys. Chem. B* **2000**, *104*, 9713–9719. [CrossRef]
36. Araujo, A.M.M.; Queiroz, G.S.; Maia, D.O.; Gondim, A.D.; Souza, L.D.; Fernandes, V.J., Jr.; Araujo, A.S. Fast Pyrolysis of Sunflower Oil in the Presence of Microporous and Mesoporous Materials for Production of Bio-Oil. *Catalysts* **2018**, *8*, 261. [CrossRef]
37. Araujo, A.S.; Jaroniec, M. Determination of the surface area and mesopore volume for lanthanide-incorporated MCM-41 materials by using high resolution thermogravimetry. *Thermochim. Acta* **2000**, *345*, 173–177. [CrossRef]
38. Barros, J.M.F.; Fernandes, G.J.T.; Araujo, M.D.S.; Melo, D.M.A.; Gondim, A.D.; Fernandes, V.J., Jr.; Araujo, A.S. Hydrothermal Synthesis and Properties of Nanostructured Silica Containing Lanthanide Type Ln-SiO<sub>2</sub> (Ln = La, Ce, Pr, Nd, Eu, Gd, Dy, Yb, Lu). *Nanomaterials* **2023**, *13*, 382. [CrossRef] [PubMed]
39. Araujo, A.S.; Jaroniec, M. Synthesis and properties of lanthanide incorporated mesoporous molecular sieves. *J. Colloid. Interf. Sci.* **1999**, *218*, 462–467. [CrossRef] [PubMed]
40. Coutinho, A.C.S.L.S.; Quintella, S.A.; Araujo, A.S.; Barros, J.M.F.; Pedrosa, A.M.G.; Fernandes, V.J., Jr.; Souza, M.J.B. Thermogravimetry applied to characterization of SBA-15 nanostructured material. *J. Therm. Anal. Calorim.* **2007**, *87*, 457–461. [CrossRef]
41. Souza, M.J.B.; Silva, A.O.S.; Aquino, J.M.F.B.; Fernandes, V.J., Jr.; Araujo, A.S. Kinetic study of template removal of MCM-41 nanostructured material. *J. Therm. Anal. Calorim.* **2004**, *75*, 693–698. [CrossRef]
42. Araujo, A.S.; Fernandes, V.J., Jr.; Souza, M.J.B.; Silva, A.O.S.; Aquino, J.M.F.B. Model free-kinetics applied to CTMA+ removal of AlMCM-41 molecular sieves. *Thermochim. Acta* **2004**, *413*, 235–2408. [CrossRef]
43. Araujo, S.A.; Ionashiro, M.; Fernandes, V.J., Jr.; Araujo, A.S. Thermogravimetric investigations during the synthesis of silica-based MCM-41. *J. Therm. Anal. Calorim.* **2001**, *64*, 801–805. [CrossRef]
44. Souza, M.J.B.; Lima, S.H.; Araujo, A.S.; Pedrosa, A.M.G.; Coutinho, A.C.S.L.S. Determination of the acidity of MCM-41 with different Si/Al ratios by the temperature programmed desorption of pyridine. *Ads. Sci. Techn.* **2007**, *25*, 751–756. [CrossRef]
45. Araujo, A.S.; Souza, C.D.R.; Souza, M.J.B.; Fernandes, V.J., Jr.; Pontes, L.A.M. Acid properties of ammonium exchanged AlMCM-41 with different Si/Al ratio. *Stud. Surf. Sci. Catal.* **2002**, *141*, 467–472.
46. Farias, M.F.; Domingos, Y.S.; Fernandes, G.J.T.; Castro, F.L.; Fernandes, V.J., Jr.; Costa, M.J.F.; Araujo, A.S. Effect of acidity in the removal-degradation of benzene in water catalyzed by Co-MCM-41 in medium containing hydrogen peroxide. *Microp. Mesop. Mater.* **2018**, *258*, 33–40. [CrossRef]
47. Coriolano, A.C.F.; Barbosa, G.F.S.; Alberto, C.K.D.; Delgado, R.C.O.B.; Castro, K.K.V.; Araujo, A.S. Catalytic processing of atmospheric residue of petroleum over AlSBA-15 nanomaterials with different acidity. *Petrol. Sci. Techn.* **2016**, *34*, 627–632. [CrossRef]
48. Gajardo, J.; Colmenares-Zerpa, J.; Peixoto, A.F.; Silva, D.S.A.; Silva, J.A.; Gispert-Guirado, F.; Llorca, J.; Chimentão, R.J. Revealing the effects of high Al loading incorporation in the SBA-15 silica mesoporous material. *J. Porous Mat.* **2023**, *5*, 1687–1707. [CrossRef]
49. Fernandes, V.J., Jr.; Araujo, A.S.; Fernandes, G.J.T. Thermal analysis applied to solid catalysts. Acidity, activity and regeneration. *J. Therm. Anal. Calorim.* **1999**, *56*, 275–285. [CrossRef]
50. Zhao, D.; Hou, Q.; Feng, J.; Chmelka, B.F.; Stucky, G.D. Nonionic triblock and star diblock copolymer and oligomeric surfactant syntheses of highly ordered, hydrothermally stable, mesoporous silica structures. *J. Am. Chem. Soc.* **1998**, *120*, 6024–6036. [CrossRef]
51. Zhao, D.; Feng, J.; Hou, Q.; Melosh, N.; Fredrickson, G.H.; Chmelka, B.F.; Stucky, G.D. Triblock copolymer syntheses of mesoporous silica with periodic 50 to 300 angstrom pores. *Science* **1998**, *279*, 548–552. [CrossRef]
52. Han, Y.J.; Kim, J.M.; Stucky, G.D. Preparation of noble metal nanowires using hexagonal mesoporous silica SBA-15. *Chem. Mater.* **2000**, *12*, 2068–2069. [CrossRef]
53. Dhar, G.M.; Kumar, G.M.; Kumar, M.; Rawat, K.S.; Sharma, L.D.; Raju, B.D.; Rao, K.S.R. Physico-chemical characterization and catalysis on SBA-15 supported molybdenum hydrotreating catalysts. *Catal. Today* **2005**, *99*, 309–314. [CrossRef]
54. Kumaran, G.M.; Garg, S.; Soni, K.; Kumar, M.; Sharma, L.D.; Dhar, G.M.; Rao, K.S.R. Effect of Al-SBA-15 support on catalytic functionalities of hydrotreating catalysts I. Effect of variation of Si/Al ratio on catalytic functionalities. *Appl. Catal. A Gen.* **2006**, *305*, 123–129.
55. Tuel, A.; Hubert-Pfalzgraf, L.G. Nanometric monodispersed titanium oxide particles on mesoporous silica: Synthesis, characterization and catalytic activity in oxidation reactions in the liquid phase. *J. Catal.* **2003**, *217*, 343–353. [CrossRef]
56. ICDD (International Center for Diffraction Data) and JCPDS (Joint Committee on Powder Diffraction Standards). Available online: <http://www.icdd.com/> (accessed on 20 February 2024).
57. Thommes, M.; Kaneko, K.; Neimark, A.V.; Olivier, J.P.; Rodriguez-Reinoso, F.; Rouquerol, J.; Sing, K.S.W. Physisorption of Gases, with Special Reference to the Evaluation of Surface Area and Pore Size Distribution (IUPAC Technical Report). *Pure Appl. Chem.* **2015**, *87*, 1051–1069. [CrossRef]
58. Brunauer, S.; Emmett, P.H.; Teller, E. Adsorption of gases in multimolecular layers. *J. Am. Chem. Soc.* **1938**, *60*, 309–319. [CrossRef]

59. Barrett, E.P.; Joyner, L.G.; Halenda, P.P. The determination of pore volume and area distributions in porous substances. I. Computations from nitrogen isotherms. *J. Am. Chem. Soc.* **1951**, *73*, 373–380. [[CrossRef](#)]
60. Eswaramoorthi, I.; Dalai, A.K. Synthesis, characterization and catalytic performance of boron substituted SBA-15 molecular sieves. *Microp. Mesop. Mat.* **2006**, *93*, 1–11. [[CrossRef](#)]
61. Vinu, A.; Kumar, G.S.; Ariga, K.; Murugesan, V. Preparation of highly ordered mesoporous AlSBA-15 and its application to isopropylation of m-cresol. *J. Mol. Catal. A* **2005**, *235*, 57–66. [[CrossRef](#)]
62. Gédéon, A.; Lassoued, A.; Bonardet, J.L.; Fraissard, J. Surface acidity diagnosis and catalytic of AlSBA materials obtained by direct synthesis. *Microp. Mesop. Mat.* **2001**, *801*, 44–45. [[CrossRef](#)]
63. Ooi, Y.S.; Zakaria, R.; Mohamed, A.R.; Bhatia, S. Hydrothermal stability and catalytic activity of mesoporous aluminum-containing SBA-15. *Catalysis Comm.* **2004**, *5*, 441–445. [[CrossRef](#)]
64. Chao, M.C.; Lin, H.P.; Sheu, H.S.; Mou, C.Y. A study of morphology of mesoporous silica SBA-15. *Stud. Surf. Sci. Catal.* **2002**, *141*, 387–394.
65. Choi, D.G.; Yang, S.M. Effect of two-step sol-gel reaction on the mesoporous silica structure. *J. Colloid Interf. Sci.* **2003**, *261*, 127–132. [[CrossRef](#)] [[PubMed](#)]
66. Katiyar, A.; Yadav, S.; Smirniotis, P.; Pinto, N.G. Synthesis of ordered large pore SBA-15 spherical particles for adsorption of biomolecules. *J. Chromatogr. A* **2006**, *1*, 13–20. [[CrossRef](#)]
67. Wang, E.; Yang, F.; Song, M.; Chen, G.; Zhang, Q.; Wang, F.; Bing, L.; Wang, G.; Han, D. Recent advances in the unsupported catalysts for the hydrodesulfurization of fuel. *Fuel Proc. Techn.* **2022**, *235*, 107386. [[CrossRef](#)]
68. Lauritsen, J.V.; Besenbacher, F. Atom-resolved scanning tunneling microscopy investigations of molecular adsorption on MoS<sub>2</sub> and CoMoS hydrodesulfurization catalysts. *J. Catal.* **2015**, *328*, 49–58. [[CrossRef](#)]
69. Tétényi, P.; Szarvas, T.; Ollár, T. Experimental proof of thiophene hydrodesulfurization reaction steps by isotope (<sup>14</sup>C) labeled thiophene. *React. Kinet. Mechan. Catal.* **2021**, *134*, 697–710. [[CrossRef](#)]
70. Desikan, P.; Amberg, C.H. Catalytic hydrodesulphurization of thiophene. Selective poisoning plus acidity of catalyst surface. *Can. J. Chem.* **1964**, *42*, 843–850.
71. Iwamoto, R.; Inamura, K.; Nozaki, T.; Lino, A. Effect of cobalt on the sulfiding temperature of CoO-MoO<sub>3</sub>/Al<sub>2</sub>O<sub>3</sub> studied by temperature programmed sulfiding. *Appl. Catal. A Gen.* **1997**, *163*, 217–225. [[CrossRef](#)]
72. Tsyganenko, A.A.; Storozheva, E.N.; Manoilova, O.V.; Lesage, T.; Daturi, M.; Lavalley, J.-C. Brønsted acidity of silica silanol groups induced by adsorption of acids. *Catal. Lett.* **2000**, *70*, 159–163. [[CrossRef](#)]
73. Wijaya, K.; Lammaduma Malau, M.L.; Utami, M.; Mulijani, S.; Patah, A.; Wibowo, A.C.; Chandrasekaran, M.; Rajabathar, J.R.; Al-Lohedan, H.A. Synthesis, Characterizations and Catalysis of Sulfated Silica and Nickel Modified Silica Catalysts for Diethyl Ether (DEE) Production from Ethanol towards Renewable Energy Applications. *Catalysts* **2021**, *11*, 1511. [[CrossRef](#)]
74. Yamada, T.; Zhou, H.; Asai, K.; Honma, I. Pore size controlled mesoporous silicate powder prepared by triblock copolymer templates. *Mater. Lett.* **2002**, *56*, 93–96. [[CrossRef](#)]

**Disclaimer/Publisher’s Note:** The statements, opinions and data contained in all publications are solely those of the individual author(s) and contributor(s) and not of MDPI and/or the editor(s). MDPI and/or the editor(s) disclaim responsibility for any injury to people or property resulting from any ideas, methods, instructions or products referred to in the content.